Glucocerebrosidases catalyze a transgalactosylation reaction that yields a newly-identified brain sterol metabolite, galactosylated cholesterol

Received for publication, December 31, 2019, and in revised form, February 18, 2020 Published, Papers in Press, March 6, 2020, DOI 10.1074/jbc.RA119.012502

Hisako Akiyama[‡§], Mitsuko Ide[§¶], Yasuko Nagatsuka[§], Tomoko Sayano[§], Etsuro Nakanishi[‖], Norihito Uemura[‖], Kohei Yuyama[**], Yoshiki Yamaguchi[‡‡], Hiroyuki Kamiguchi[‡§], Ryosuke Takahashi[‖], Johannes M. F. G. Aerts[§§], Peter Greimel[‡], and Yoshio Hirabayashi[§¶1]

From the [‡]RIKEN Center for Brain Science, [§]RIKEN Brain Science Institute, and [¶]Cellular Informatics Laboratory, RIKEN, Wako, Saitama 351-0198, Japan, the [‖]Department of Neurology, Kyoto University Graduate School of Medicine, Kyoto 606-8501, Japan, the [**]Lipid Biofunction Section, Faculty of Advanced Life Science, Hokkaido University, Sapporo, Hokkaido 001-0021, Japan, the [‡‡]Laboratory of Pharmaceutical Physical Chemistry, Tohoku Medical and Pharmaceutical University, Sendai, Miyagi 981-8558, Japan, and the [§§]Department of Medical Biochemistry, Leiden Institute of Chemistry, Leiden 2333 CC, The Netherlands

Edited by Dennis R. Voelker

β-Glucocerebrosidase (GBA) hydrolyzes glucosylceramide (GlcCer) to generate ceramide. Previously, we demonstrated that lysosomal GBA1 and nonlysosomal GBA2 possess not only GlcCer hydrolase activity, but also transglucosylation activity to transfer the glucose residue from GlcCer to cholesterol to form β-cholesterylglucoside (β-GlcChol) *in vitro*. β-GlcChol is a member of sterylglycosides present in diverse species. How GBA1 and GBA2 mediate β-GlcChol metabolism in the brain is unknown. Here, we purified and characterized sterylglycosides from rodent and fish brains. Although glucose is thought to be the sole carbohydrate component of sterylglycosides in vertebrates, structural analysis of rat brain sterylglycosides revealed the presence of galactosylated cholesterol (β-GalChol), in addition to β-GlcChol. Analyses of brain tissues from GBA2-deficient mice and GBA1- and/or GBA2-deficient Japanese rice fish (*Oryzias latipes*) revealed that GBA1 and GBA2 are responsible for β-GlcChol degradation and formation, respectively, and that both GBA1 and GBA2 are responsible for β-GalChol formation. Liquid chromatography–tandem MS revealed that β-GlcChol and β-GalChol are present throughout development from embryo to adult in the mouse brain. We found that β-GalChol expression depends on galactosylceramide (GalCer), and developmental onset of β-GalChol biosynthesis appeared to be during myelination. We also found that β-GlcChol and β-GalChol are secreted from neurons and glial cells in association with exosomes. *In vitro* enzyme assays confirmed that GBA1 and GBA2 have transgalactosylation activity to transfer the galactose residue from GalCer to cholesterol to form β-GalChol. This is the first report of the existence of β-GalChol in vertebrates and how β-GlcChol and β-GalChol are formed in the brain.

Glycosylation of lipids, including glycerolipids, sterols, and sphingolipids, is a highly-conserved system in living organisms. Sterylglycosides are glycosylated sterols that are found in bacteria, fungi, plants, and animals (1). This evolutionary conservation of sterylglycosides across domains of organisms indicates that they likely play critical roles in fundamental cellular processes. In vertebrates, cholesterol is the major sterol component, and its glucosylation forms β-cholesterylglucoside (1-*O*-cholesteryl-β-D-glucopyranoside (β-GlcChol)).[2] Recently, Marques *et al.* (2) dem-

This work was supported by the ONO Medical Research Foundation (to H. A.); research grants from the RIKEN Special Postdoctoral Research program (to H. A.); AMED under Grant JP19dm0207001 (to H. K.); JSPS KAKENHI Grants JP26860199, JP17K15608, JP17KK0147 (to H. A.), JP16K14687 (to Y. H.), and JP15H02540 (to R. T.); and The Mizutani Foundation for Glycoscience (to Y. H.). The authors declare that they have no conflicts of interest with the contents of this article.

This article contains Figs. S1–S2 and Tables S1–S2.

[1] To whom correspondence should be addressed: Cellular Informatics Laboratory, RIKEN, 2-1 Hirosawa, Wako, Saitama 351-0198, Japan. Tel.: 81-48-462-1111 (Ext. 7675); Fax: 81-48-467-9795; E-mail: hirabaya@riken.jp.

[2] The abbreviations used are: β-GlcChol, β-cholesterylglucoside or 1-*O*-cholesteryl-β-D-glucopyranoside; Alix, ALG-2-interacting protein X; BCA, bicinchoninic acid; β-GalChol, β-cholesterylgalactoside or 1-*O*-cholesteryl-β-D-galactopyranoside; β-GlcChol-d_7, deuterium-labeled β-cholesterylglucoside; β-GlcSito, β-sitosterylglucoside or 1-*O*-sitosteryl-β-D-glucopyranoside; Cas, CRISPR-associated; CBE, conduritol B epoxide or DL-1,2-anhydro-myo-inositol; ceramide (d18:1-C12:0), *N*-lauroyl-D-erythro-sphingosine; CGT, UDP-galactose:ceramide galactosyltransferase; Chol, cholesterol; CID, collision-induced dissociation; C_6-NBD–GalCer, *N*-[6-[(7-nitro-2–1,3-benzoxadiazol-4-yl)amino]hexanoyl]-β-D-galactopyranosyl-(1→1)-sphingosine; C_6-NBD–GlcCer, *N*-[6-[(7-nitro-2–1,3-benzoxadiazol-4-yl)amino]hexanoyl]-β-D-glucopyranosyl-(1→1)-sphingosine; CNS, central nervous system; CRISPR, clustered regularly-interspaced short palindromic repeats; DHB, 2, 5-dihydroxybenzoic acid; ER, endoplasmic reticulum; ESI–MS/MS, electrospray ionization tandem mass spectrometry; EV, extracellular vesicle; FBS, fetal bovine serum; E, embryonic day; P, postnatal day; GALC, galactocerebrosidase or galactosylceramidase; GalCer, galactosylceramide; GalCer (d18:1-C12:0), β-D-galactopyranosyl-(1→1)-*N*-lauroyl-D-*erythro*-sphingosine; GalSph, β-D-galactopyranosyl-(1→1)-D-*erythro*-sphingosine or galactosylsphingosine; GBA1, lysosomal acid GCase; GBA2, nonlysosomal GCase; GCase, glucocerebrosidase or glucosylceramidase; GC/MS, gas chromatography/mass spectrometry; GD, Gaucher disease; GlcCer, glucosylceramide; GlcCer (d18:1-C12:0), β-D-glucopyranosyl-(1→1)-*N*-lauroyl-D-*erythro*-sphingosine; GlcCer (d18:1-C18:0), β-D-glucopyranosyl-(1→1)-*N*-stearoyl-D-*erythro*-sphingosine; GlcCer (d18:1-C18:1), β-D-glucopyranosyl-(1→1)-*N*-oleoyl-D-*erythro*-sphingosine; GlcSph, β-D-glucopyranosyl-(1→1)-D-*erythro*-sphingosine or glucosylsphingosine; HILIC, hydrophilic interaction chromatography; HOHAHA, homonuclear Hartmann-Hahn; HPTLC, high-performance thin layer chromatography; HRP, horseradish peroxidase; HSQC, heteronuclear single quantum coherence; KDEL, Lys–Asp–Glu–Leu, an ER retention sequence; MRM, multiple reaction monitoring; MSA, multiple system atrophy; NBD–chol, 25-NBD–cholesterol or 25-[*N*-[(7-nitro-2–1,3-benzoxadiazol-4-yl)methyl]amino]-27-norcholesterol; NBD–GalChol, 25-NBD–galactosyl-cholesterol; NB-DGJ, *N*-(*n*-butyl)deoxygalactonojirimy-

onstrated that β-GlcChol is present in human and mouse tissue, including brain, by using liquid chromatography (LC)-electrospray ionization tandem MS (ESI–MS/MS). Because purification of β-GlcChol from central nervous system (CNS) tissue has not been reported, and structural analysis based on the β-GlcChol–containing fraction has not been reported, we developed a multistep chromatographic purification protocol capable of isolating β-GlcChol from the brain, an organ that contains high levels of glucosylceramide (GlcCer) and galactosylceramide (GalCer). As they exhibit very similar chromatographic behavior to β-GlcChol, a method like ours is needed to differentiate it from GlcCer and GalCer. Although β-GlcChol is thought to be the sole sterylglycoside in vertebrates, in embryonic chicken brain we found two more sterylglucosides, the plant-type β-sitosterylglucoside (1-*O*-sitosteryl-β-D-glucopyranoside (β-GlcSito)) and an as-of-yet structurally- and not fully-identified homologue termed GSX-2 (3). Available structural information on GSX-2 suggests high similarity with plant-type β-campesterylglucoside (1-*O*-campesteryl-β-D-glucopyranoside) (3).

Formation of β-GlcChol is mediated by glucocerebrosidase (GCase, GlcCer-degrading β-glucosidase) 1 and 2 (GBA1 and GBA2). GBA1 (lysosomal acid GCase, EC 3.2.1.45) is a water-soluble enzyme that can associate with lysosomal membranes. Homozygous mutations in the *GBA1* gene cause Gaucher disease (GD), which is the most common lysosomal storage disorder. It is characterized by the accumulation of GlcCer in the lysosomal compartment of macrophages (4, 5). Heterozygous mutations in the *GBA1* gene are a high-risk factor for Parkinson's disease (PD) and multiple system atrophy (MSA) (6, 7). GBA2 (nonlysosomal GCase, EC 3.2.1.45) is a nonintegral membrane-associated protein that localizes at the cytosolic surface of the endoplasmic reticulum (ER) and Golgi apparatus (8–11). GBA2-deficient mice accumulate GlcCer in the testis, brain, and liver, and they exhibit male infertility (9) and delayed liver regeneration (12). Loss– of–function mutations in the *GBA2* gene cause neurological disorders, such as cerebellar ataxia and spastic paraplegia (13–15). In mammalian cells *in vitro*, both GBA1 and GBA2 possess not only GlcCer hydrolase activity but also transferase activity, catalyzing a transglucosylation reaction to form β-GlcChol via transfer of the glucose residue from GlcCer to cholesterol (2, 16). GBA1 and GBA2 also possess β-GlcChol hydrolase activity, and both enzymes can transfer a glucose residue from β-GlcChol to ceramide, indicating that the enzymes catalyze a reversible transglucosylation reaction between GlcCer and β-GlcChol via a glucose molecule (2, 16).

The concentration of β-GlcChol is elevated in the liver and the plasma of a GD mouse model. It is also elevated in the plasma of GD patients, the liver of a Niemann-Pick disease type C (NPC) disease mouse model, and the plasma of NPC patients (2). β-GlcChol also increases in cells treated with U18666A, an amphiphilic compound that inhibits cholesterol transport and causes accumulation of cholesterol in lysosomes. U18666A-induced β-GlcChol elevation is inhibited by conduritol B epoxide (DL-1,2-anhydro-myo-inositol; CBE), a specific inhibitor of GBA1 (2). GBA2-deficient mice have decreased levels of β-GlcChol in the thymus, the liver, and plasma (2), suggesting that GBA2 is responsible for β-GlcChol formation *in vivo*. Under normal conditions, GBA1 and GBA2 seem to contribute to β-GlcChol degradation and formation, respectively. In contrast, when excess cholesterol accumulates in lysosomes, such as that found in NPC disease, GBA1 actively generates β-GlcChol (2). Although β-GlcChol metabolism mediated by GBA1 and GBA2 has been studied in several kinds of cells and tissues and in plasma, the metabolism of sterylglycosides in the brain is not understood.

Although glucose is considered as the sole carbohydrate headgroup in vertebrate sterylglycosides, we previously reported the presence of a sterylglycoside constituent from brain and sciatic nerve tissue exhibiting resistance against digestion by recombinant human GBA1 (rGBA1), Cerezyme® (2, 3). In contrast, GSX-2 and β-GlcSito fractions from embryonic chicken brains (E6 to E18) were digested completely by rGBA1 (3).

In this report, we describe the isolation of sterylglycosides from 12-week-old rat brains, as previous reports suggested a higher content of the rGBA1-resistant sterylglycosides in adult brains compared with early-stage embryonic brains (2, 3). Structural analysis of the isolated sterylglycoside fractions revealed the presence of β-cholesterylgalactoside (1-*O*-cholesteryl-β-D-galactopyranoside, β-GalChol), in addition to β-GlcChol, GSX-2, and β-GlcSito. To understand the biological significance of brain sterylglycosides, we determined their developmental expression and cellular distribution. Using the brains of GBA2-deficient mice and GBA1- and/or GBA2-deficient *Oryzias latipes* (also known as Japanese rice fish or medaka), we demonstrated that GBA1 is involved in β-GlcChol degradation and β-GalChol formation and that GBA2 is involved in the formation of β-GlcChol and β-GalChol and degradation of GSX-2 and β-GlcSito *in vivo*. It has not been reported that GBA1 and GBA2 have GalCer-degrading β-gal activity. However, our *in vitro* enzyme assays revealed that GBA1 and GBA2 degraded GalCer and synthesized β-GalChol from GalCer and cholesterol. Our work described here is the first report to demonstrate the existence of β-GalChol in vertebrates and to demonstrate the metabolism of sterylglycosides in vertebrate brain.

Results

Previously unidentified cholesterylglucoside-related lipid in adult rodent brain

A sterylglycosides fraction was enriched and isolated from CNS tissues using a previously developed multistep chromatographic purification protocol (3). The glycerophospholipid fraction was hydrolyzed, and then sterylglycosides were enriched by normal phase chromatography. We used a chloroform/methanol (C/M) gradient for normal-phase chromatography. For reversed-phase (RP) chromatography, we used a

cin; NBD–GlcChol, 25-NBD– glucosyl-cholesterol; NPC, Niemann Pick disease type C; PD, Parkinson's disease; rGALC, recombinant human galactosylceramidase; rGBA1, recombinant human GBA1; RP, reversed-phase; SM, sphingomyelin; SM (d18:1-C12:0), *N*-lauroyl-D-*erythro*-sphingosylphosphorylcholine; TMS, *N*-methyl-*N*-(trimethylsilyl) trifluoroacetamide; TXI, triple-resonance; U18666A, (3β)-3-[2-(diethylamino)ethoxy]androst-5-en-17-one hydrochloride; UDP-Gal, UDP-galactose or uridine 5′-diphosphogalactose disodium salt; UDPG-SGTase, UDP-glucose:sterol glucosyltransferase; UGCG, GlcCer synthase or UDP-glucose:ceramide glucosyltransferase; C/M, chloroform/methanol; M/W, methanol/water; n.r., not resolved.

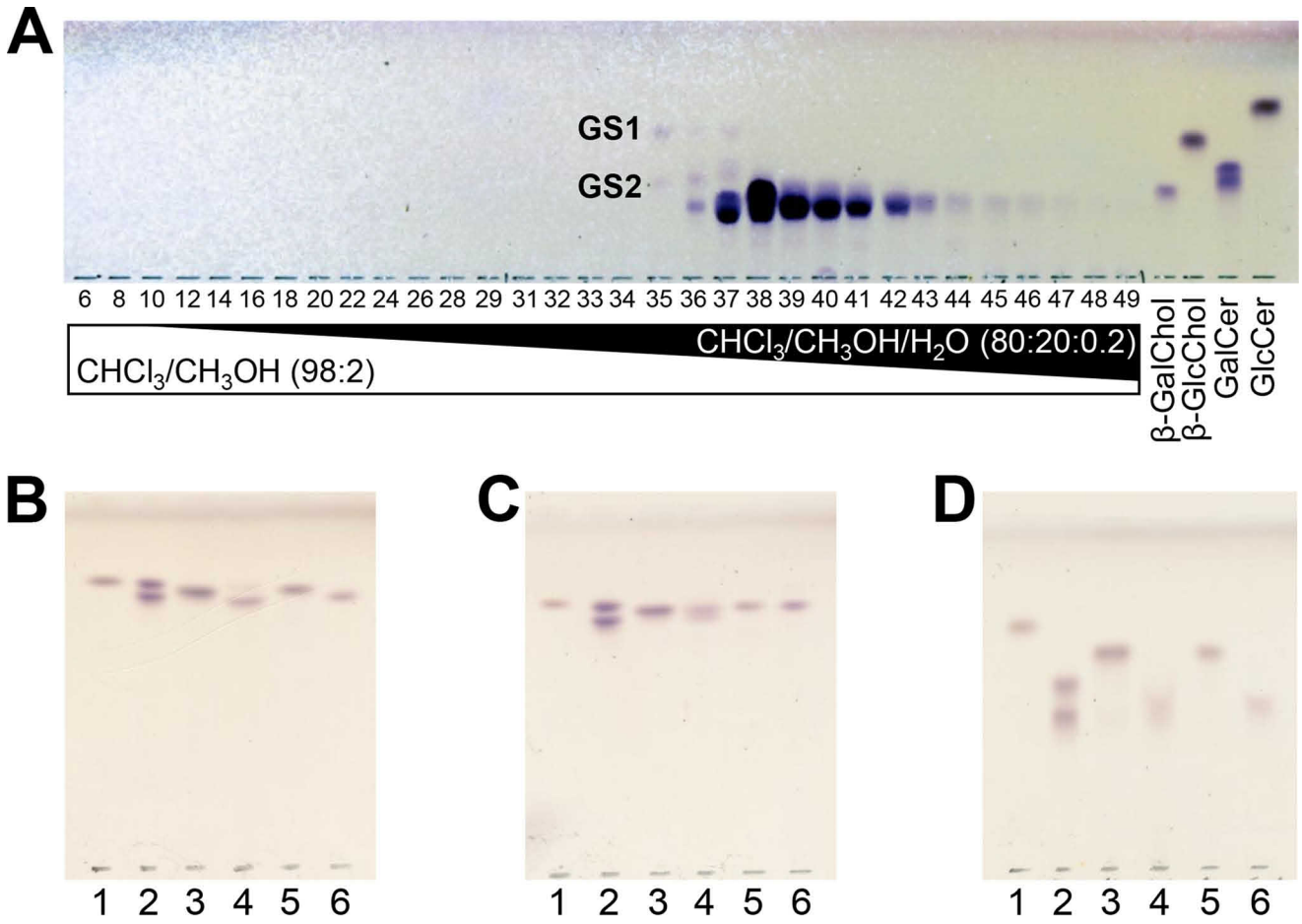

Figure 1. Purification of sterylglycosides from 12-week-old rat brains. *A,* HPTLC analysis of the sterylglycoside elution profile from a silica gel column during enrichment, visualized by orcinol staining. The bands co-migrating with standard β-GlcChol and β-GalChol in fraction 35 are designated *GS1* and *GS2*, respectively; each was collected for further purification. *B–D*, HPTLC mobilities of isolated GS1 and GS2 fractions using C/M/W (65:35:8, v/v/v) as a solvent system with Silica Gel 60 (*B*); C/M/W (65:35:8, v/v/v) as a solvent system with Silica Gel 60 impregnated with 1% boric acid (*C*); and hexane/isopropyl alcohol/C/M/W (25:35:65:25:3, v/v/v/v/v) as a solvent system with Silica Gel 60 impregnated with 1% boric acid (*D*). Lipids were visualized with orcinol staining. *Lane 1*, GlcCer (d18:1-C18:0); *lane 2*, GalCer from bovine brain; *lane 3*, GS1 fraction purified from rat brains; *lane 4*, GS2 fraction purified from rat brains; *lane 5,* authentic β-GlcChol standard; and *lane 6*, authentic standard of β-GalChol.

methanol/water (M/W) gradient. To remove the large excess of GalCer that was enriched together with sterylglycosides, we performed normal-phase chromatography again using a C/M gradient (Fig. 1*A*). Analysis of boronated high-performance TLC (HPTLC) revealed that the GalCer fraction was successfully separated. The bands co-migrating with standard β-GlcChol and β-GalChol in fraction 35 were each collected, extracted, and designated as GS1 and GS2, respectively. HPTLC mobility of GS1 and GS2 under different developmental conditions (Fig. 1, *B–D*) revealed a single orcinol-reactive spot co-migrating with authentic β-GlcChol standard for GS1. GS2 exhibited one or two spots visualized by orcinol, and the mobility of the major spot corresponded to that of the authentic β-GalChol standard.

NMR analysis of GS1 and GS2 revealed a characteristic pattern in the range of 4.5–3.3 ppm (Fig. 2*A*), which is typically associated with glucopyranosides and galactopyranosides, respectively. The ^{1}H chemical shifts of the hexoside portion matches well with those of the references (Table S1). The large splittings (7.7 and 6.9 Hz) of the anomeric protons (Glc H-1 and Gal H-1) at 4.43 and 4.38 ppm in GS1 and GS2, respectively, are archetypical for an axial–axial *J* coupling consistent with β-glycosidic linkage. In the low-field region, the aglycon exhibits a deshielded vinyl proton at 5.4 ppm (Chol H-6), which is consistent with the presence of a Chol C5–C6 double bond. The high-field region of the ^{1}H–^{13}C HSQC spectrum of GS1 (Fig. 2*B*) confirms the presence of the expected β-cholesteryl aglycon. The carbohydrate region of the homonuclear Hartmann-Hahn (HOHAHA) spectrum of GS2 confirmed the presence of galactopyranoside (Fig. 2*C*).

To gain further structural insight of the main constituents in GS1 and GS2, each fraction was subjected to reversed-phase LC (RPLC)-ESI–MS/MS analysis. A neutral-loss scan of the carbohydrate moiety following collision-induced dissociation (CID) revealed a single peak for each sample corresponded to a parent ion $[M + NH_4]^+$ at *m/z* 566 (Fig. 3, *A* and *B*). The peak in GS1 and GS2 exhibited similar elution time compared with authentic β-GlcChol and β-GalChol standards, respectively. MALDI-TOF/TOF analysis of the lithium adduct of GS1 and GS2 main constituents at $[M + Li]^+$ *m/z* 555.4 (Fig. 3, *C* and *D*) followed by high-energy CID (Fig. 3, *E* and *F*) revealed a dominant ion at *m/z* 187 in the product ion spectra, corresponding to [hexose + Li]$^+$. These results revealed the presence of glycosylated sterols in GS1 and GS2 fractions.

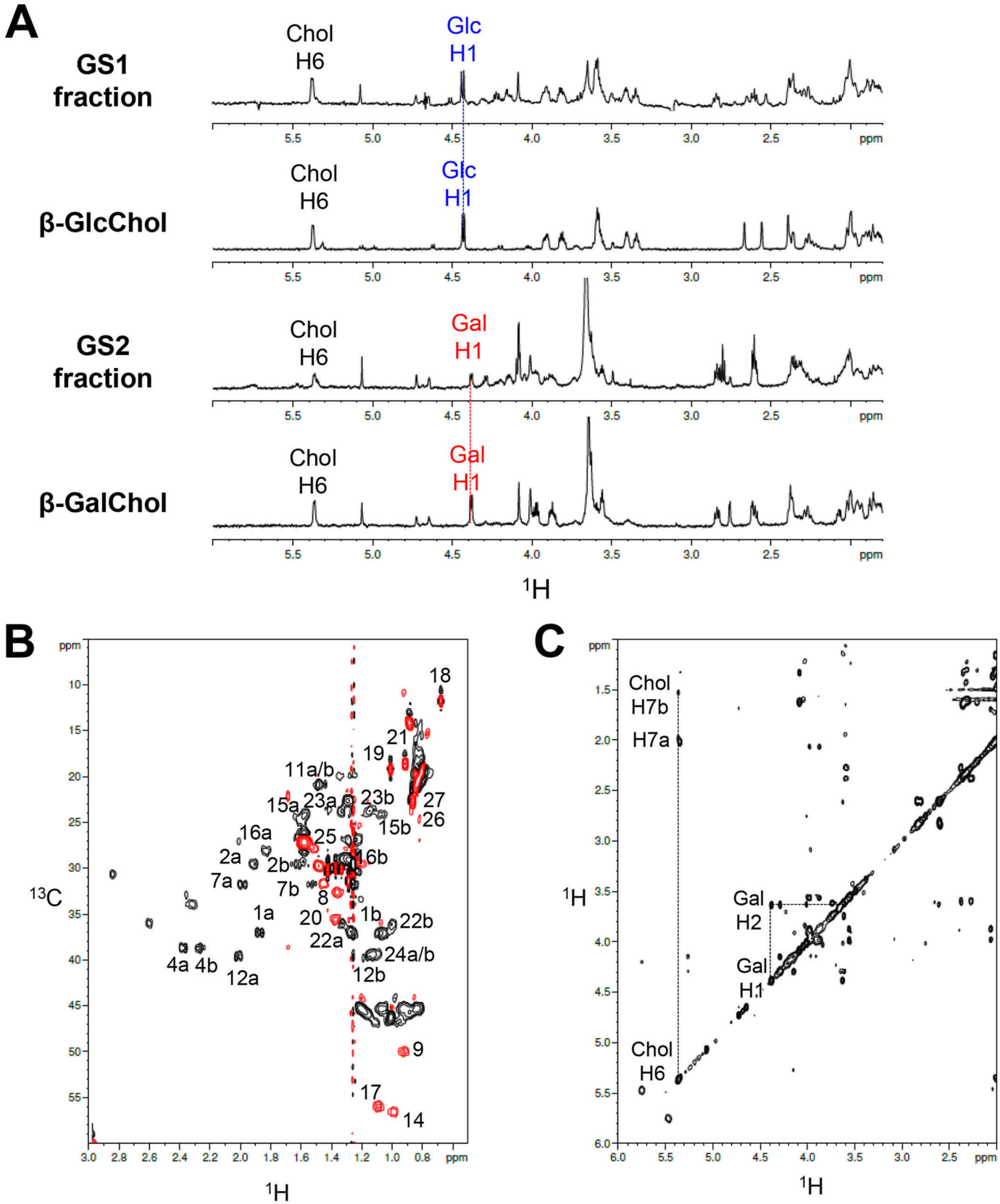

Figure 2. NMR analysis of GS1 and GS2 fractions isolated from brains of 12-week-old rats. *A,* ^{1}H NMR spectra of GS1 fraction, GS2 fraction, authentic *β*-GlcChol standard, and authentic *β*-GalChol standard. *B,* two-dimensional (2D) multiplicity-edited ^{1}H-^{3}C HSQC spectrum (CH_3, CH, *red*; CH_2, *black*) of the GS1 fraction. *C,* two-dimensional HOHAHA spectrum of GS2 fraction. Mixing time was set to 20 ms.

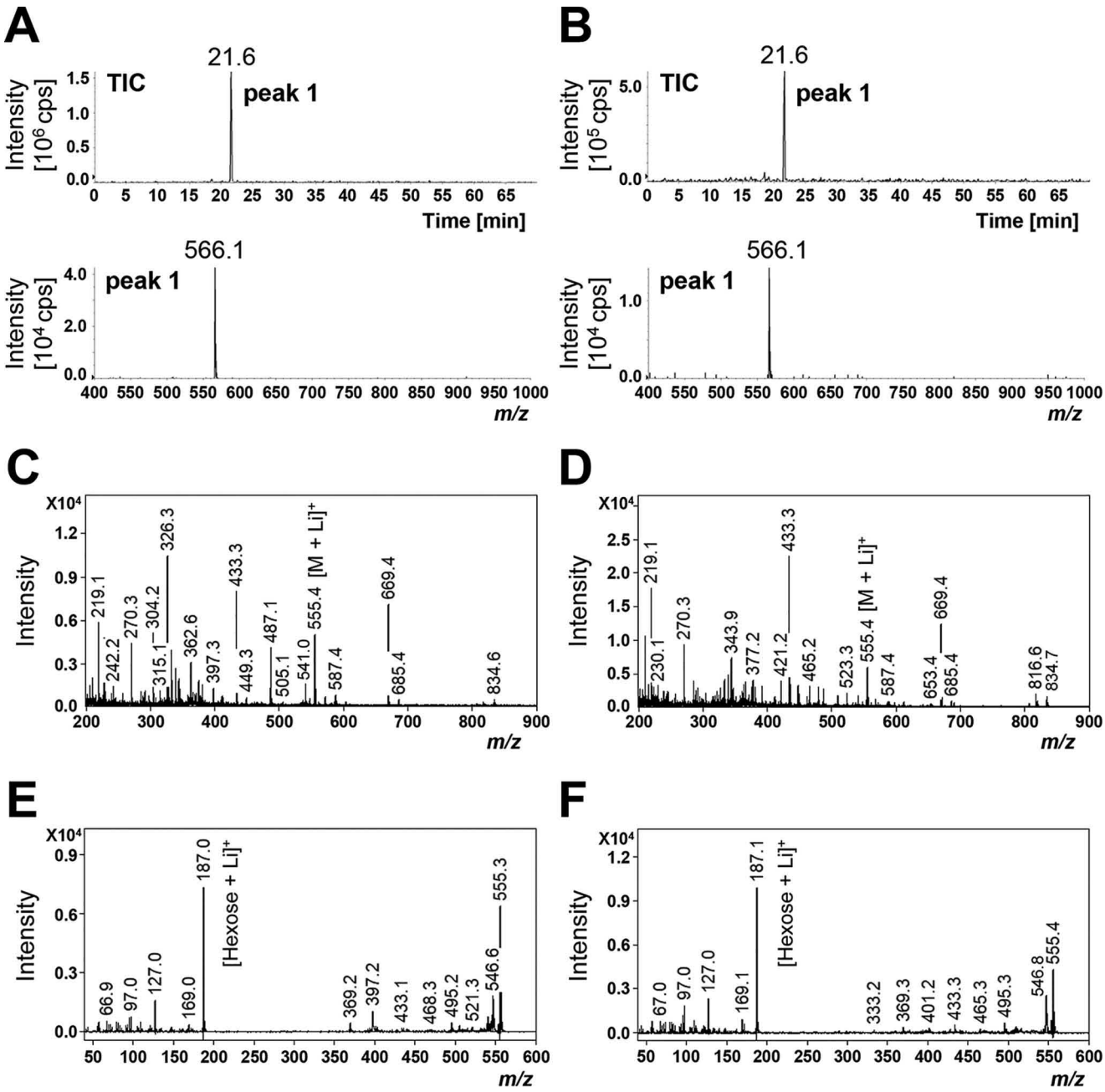

Figure 3. MS analysis of GS1 and GS2 fractions isolated from brains of 12-week-old rats. *A* and *B*, RPLC–ESI–MS/MS spectrum of GS1 (*A*) and GS2 (*B*) fractions during neutral-loss scan of $[M + NH_4]^+$. Total ion count (*TIC*) chromatogram and individual MS/MS spectra of indicated peaks are shown. *C–E*, analysis of GS1 and GS2 fractions by MALDI-TOF/TOF in positive-ion mode. MS1 spectra of GS1 fraction (*C*) and GS2 fraction (*D*). High-energy CID MS/MS spectra of GS1 fraction (*E*) and GS2 fraction (*F*) show selected precursor ion $[M + Li]^+$ *m/z* 555.4.

To determine the aglycon structure in GS1 and GS2, each fraction was subjected to enzymatic deglycosylation, followed by GC/MS (GC/MS) of the liberated aglycons (Fig. S1). The major sterol liberated from fractions GS1 and GS2 eluted at 20.2 min (Fig. S1, *A*, *peak 1*, and *D*, *peak 2*). The elution time and fragmentation pattern of the major sterol (Fig. S1, *B* and *E*) coincided well with authentic cholesterol. The liberated aglycons from fraction GS2 exhibited an additional peak eluting at 27.2 min (Fig. S1*D*, *peak 3*). The absence of the *m/z* 129 fragment (Fig. S1*F*), usually present in Δ^5-3-hydroxysteroid TMS derivatives (17), and the late elution time of peak 3 did not allow its identification.

Taken together, structural analysis of the fraction GS1 from adult rat brains confirmed the presence of β-GlcChol, and fraction GS2 revealed the presence of β-GalChol.

Characterization of sterylglycosides in brain

To characterize the expression pattern of brain sterylglycosides, we developed an analytical method using LC-MS. First, β-GalChol was chemically synthesized according to the method described under "Experimental procedures." Hexosylcholesterol, including β-GlcChol and β-GalChol, was monitored using hydrophilic interaction chromatography (HILIC)-ESI–MS/MS. HILIC columns, which are widely used for

separating glycosphingolipids (18, 19), were effective for separating β-GlcChol and β-GalChol (Fig. 4*A*).

In mouse brain lipid samples, HILIC–ESI–MS/MS detected two peaks that exhibited similar retention times as authentic standards of β-GlcChol and β-GalChol. These peaks were consistent with the peaks for β-GlcChol and β-GalChol in adult rat brain samples. HILIC–ESI–MS/MS revealed that β-GlcChol and β-GalChol differ in ionization efficiency (Fig. 4*B*). This contrasts with the ionization efficiency of GlcCer and GalCer, which was nearly the same (data not shown). To accurately quantify sterylglycosides, we used a deuterium-labeled β-GlcChol (β-GlcChol-d_7) in further experiments in order to normalize the extraction efficiency of β-GlcChol and β-GalChol. Because the ionization efficiency of β-GlcChol and β-GalChol is different, we quantified β-GlcChol and β-GalChol separately using standard curves of β-GlcChol-d_7 and β-GalChol, respectively.

To monitor the developmental expression of sterylglycosides in the brain, we used HILIC–ESI–MS/MS to analyze brain lipid extracts obtained from mice of different ages, *i.e.* embryonic day (E) 12 to postnatal week 10. The lipid extracts were added to internal standards, β-GlcChol-d_7 and GlcCer (d18:1-C12:0). Multiple reaction monitoring (MRM) analysis revealed that β-GlcChol and β-GalChol were present throughout development and varied depending on age (Fig. 5). The amount of β-GlcChol detected in E12 mouse brain was four times greater than that of β-GalChol. In contrast to the modest increase of β-GlcChol during early development, the amount of β-GalChol substantially increased after postnatal day (P) 10. Thus, at postnatal weeks 4 and 10, the concentrations of β-GlcChol and β-GalChol in mouse brain were comparable.

GlcCer and GalCer were monitored along with the sterylglycosides. The amount of GlcCer detected in E12 mouse brain was 90 times higher than that of β-GlcChol. GlcCer content decreased during development, whereas β-GlcChol slightly increased. This means that the GlcCer content in a 10-week-old postnatal mouse brain was four times greater than the β-GlcChol content. As with β-GalChol levels, the amount of GalCer (d18:1-C18:0) and GalCer (d18:1-C24:1) increased substantially after P10, suggesting β-GalChol expression relates to GalCer with long-chain fatty acid (>18 carbon atoms).

Next, we investigated the distribution of brain sterylglycosides. We previously reported that in the lipid raft fraction of human fibroblasts, β-GlcChol is formed through transglucosylation (20). The lipid composition of lipid rafts is similar to that of exosomes, extracellular vesicles (EVs) ranging in size from 70 to 150 nm in diameter (21–24). This prompted us to investigate whether sterylglycosides are released from cells via exosomes. EVs containing exosomes were prepared from the culture media of human neuroglioma H4 cells and mouse primary cortical neurons by a sequential centrifugation. The resulting 100,000 × *g* pellet was separated by continuous sucrose density gradient centrifugation. The exosomal proteins Alix, tumor susceptibility gene 101 protein, and flotillin-1 were detected in sucrose density fractions corresponding to a density range of 1.07–1.18 g/ml (Fig. 6, *A* and *D*), similar to previous reports (25, 26). We did not detect a marker protein for Golgi and an ER retention sequence in the pellet GM130 and Lys–Asp–Glu–Leu (abbreviated KDEL), respectively.

Analysis of exosomal particle size revealed that the subcellular material in the pellet contained mainly small membrane vesicles of 70–150 nm in diameter (Fig. 6, *B* and *E*). The concentrations of sterylglycosides, ceramide, sphingomyelin (SM), GlcCer, and GalCer were analyzed by LC–ESI–MS/MS (Fig. 6, *C* and *F*). Consistent with previous reports (23, 24), exosomes derived from H4 cells and mouse primary cortical neurons exhibited higher concentrations of GlcCer and GalCer compared with their cells of origin (Fig. 6, *C* and *F*). Although ceramide and SM are reportedly enriched with exosomes (21, 23, 24, 27), we only detected enrichment of ceramide in exosomes derived from H4 cells but not from mouse primary cortical neurons, and SM was not enriched in exosomes (Fig. 6, *C* and *F*). Interestingly, β-GlcChol, β-GalChol, and β-GlcSito were detected in exosomes derived from H4 cells and mouse primary cortical neurons. β-GlcChol was enriched in exosomes derived from H4 cells, whereas β-GlcSito was enriched in exosomes derived from both H4 cells and mouse primary cortical neurons (Fig. 6, *C* and *F*). GSX-2 content was below the detection threshold in all analyzed exosomes and their cells of origin.

Brain sterylglycosides are metabolized by GBA1 and GBA2 in vivo

The metabolism of sterylglycosides has been described in various tissues, but not in brain tissue. Thus, we investigated the involvement of GBA1 and GBA2 in sterylglycoside metabolism. We used the brains of GBA2-deficient ($Gba2^{-/-}$) mice and GBA1- and/or GBA2-deficient medakas (*O. latipes*) for this study.

PCR-based genotyping of mice was used to identify $Gba2^{+/+}$ and $Gba2^{-/-}$ homozygous offspring (Fig. 7*A*). The concentrations of sterylglycosides, GlcCer, and GalCer in the brains of WT and $Gba2^{-/-}$ mice were analyzed by HILIC–ESI–MS/MS (Fig. 7*B*). In the brains of $Gba2^{-/-}$ mice, β-GlcChol levels were decreased. This is consistent with the down-regulation of β-GlcChol observed in the liver, thymus, and plasma of GBA2-deficient mice (2). Unexpectedly, β-GalChol levels were also decreased in the brains of $Gba2^{-/-}$ mice. GSX-2 and β-GlcSito levels, however, were increased. To date, the levels of GlcCer and GalCer in the brains of $Gba2^{-/-}$ mice have not been reported. Our analysis showed that the level of GlcCer but not GalCer was increased in the brains of $Gba2^{-/-}$ mice. This is consistent with the finding that in $Gba2^{-/-}$ mice GlcCer is up-regulated in the testis, liver, kidney, and small intestine (9, 19).

GBA1- and/or GBA2-deficient medakas were generated by crossing $Gba1^{+/-}/Gba2^{+/-}$ heterozygous mutants.[3] The resulting offspring had one of nine possible genotypes: $Gba1^{+/+}/Gba2^{+/+}$ (WT); $Gba1^{+/-}/Gba2^{+/+}$; $Gba1^{-/-}/Gba2^{+/+}$; $Gba1^{+/+}/Gba2^{+/-}$; $Gba1^{+/-}/Gba2^{+/-}$; $Gba1^{-/-}/Gba2^{+/-}$; $Gba1^{+/+}/Gba2^{-/-}$; $Gba1^{+/-}/Gba2^{-/-}$; and $Gba1^{-/-}/Gba2^{-/-}$. HILIC–ESI–MS/MS was used to determine the concentrations of sterylglycosides in medaka brains of each of the nine geno-

[3] E. Nakanishi, N. Uemura, H. Akiyama, M. Kinoshita, H. Yamakado, S. Takeda, Y. Hirabayashi, and R. Takahashi, submitted for publication.

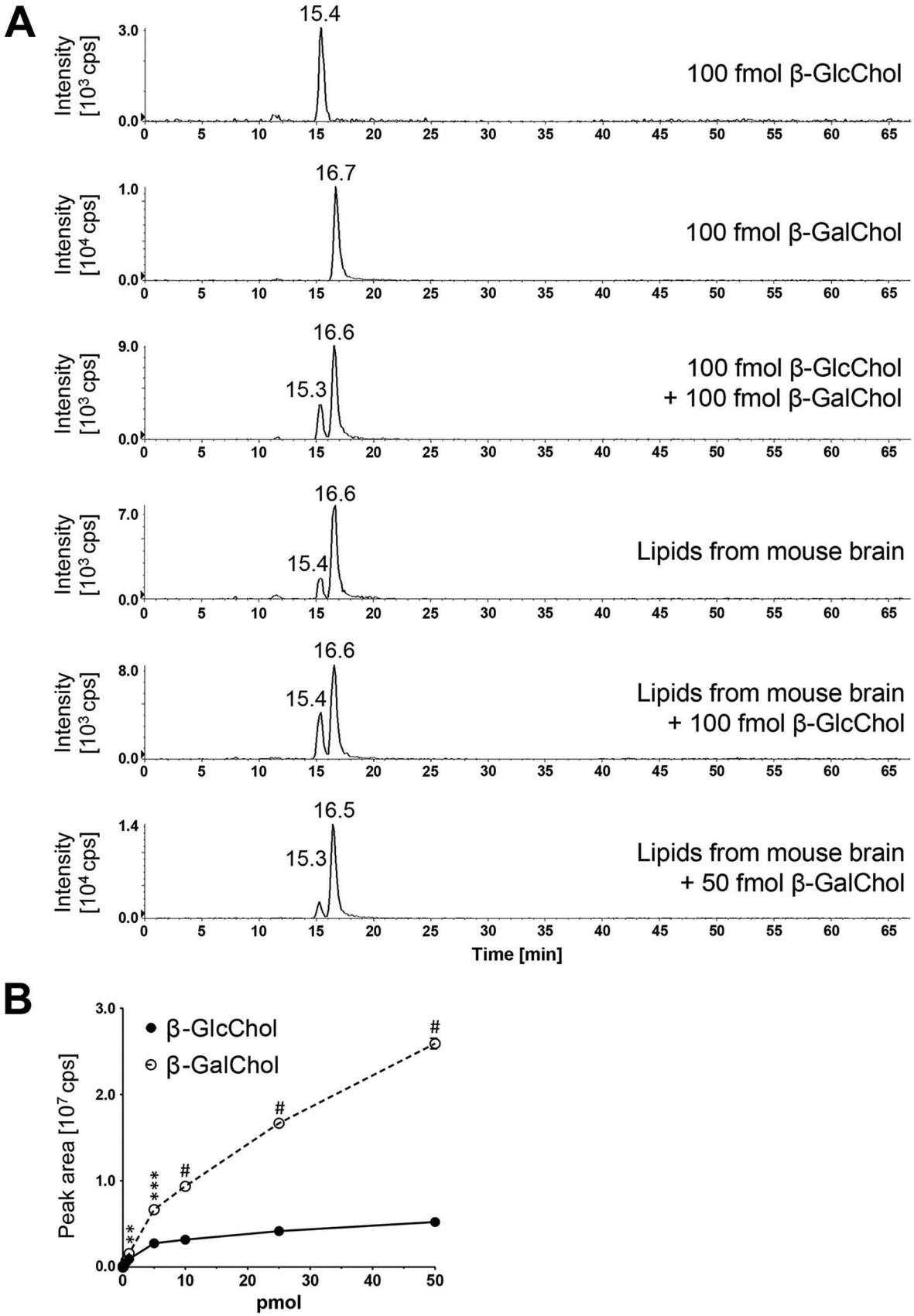

Figure 4. Quantification of β-GlcChol and β-GalChol by HILIC–ESI–MS/MS. *A,* elution pattern of β-GlcChol and β-GalChol from HILIC. Authentic standards of β-GlcChol and β-GalChol and lipids extracted from the brain of a 10-week-old C57BL/6J male mouse were analyzed by HILIC–ESI–MS/MS. Monitored precursor–product ion pair was 566/369. *B,* different concentrations of authentic standards of β-GlcChol and β-GalChol were analyzed using HILIC–ESI–MS/MS, and peak areas were integrated. Data ($n = 3$) are means ± S.E. Differences were analyzed by unpaired *t* tests. **, $p < 0.01$; ***, $p < 0.001$; #, $p < 0.0001$.

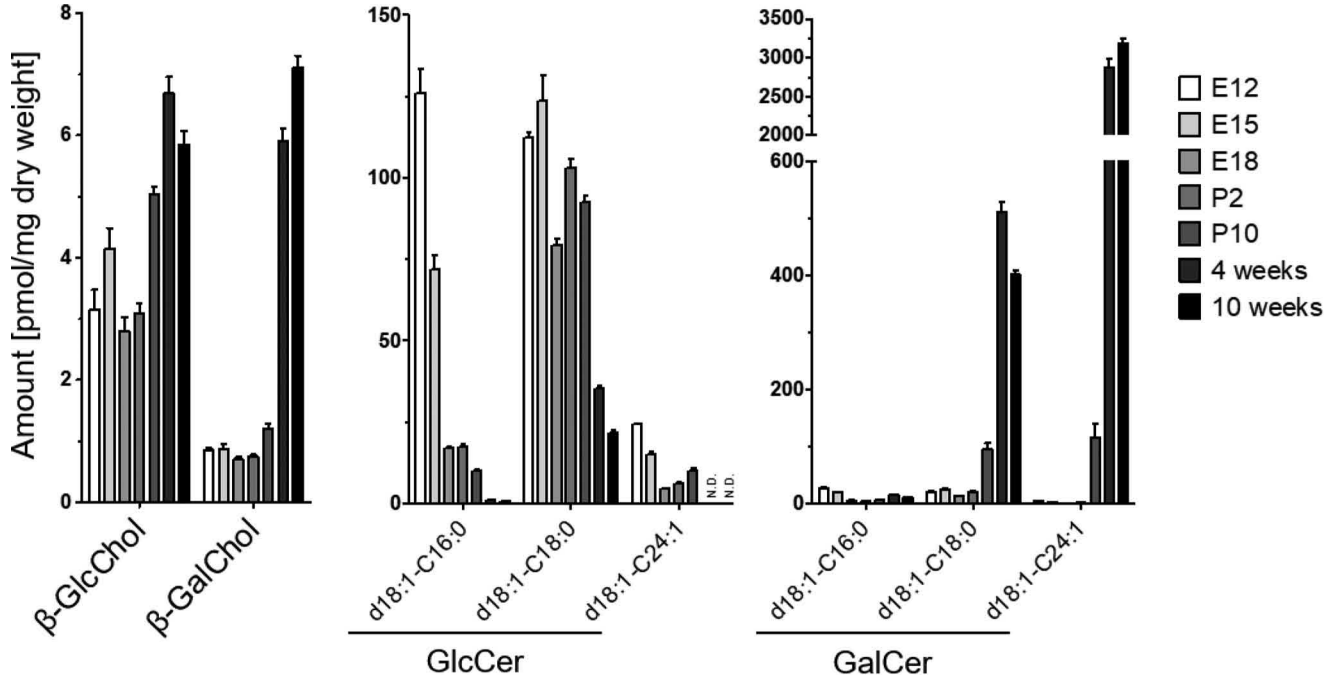

Figure 5. Concentrations of sterylglycosides and selected species of GlcCer and GalCer in mouse brain at the indicated developmental stages. Data (n = 3–5) are means ± S.E. *N.D.*, not detected (below the detection threshold).

types (Fig. 7*C*). In *Gba1*$^{-/-}$/*Gba2*$^{+/+}$ medakas, β-GlcChol levels were increased in the brains. This was consistent with the finding that β-GlcChol is up-regulated in the liver and plasma of GBA1-deficient mice (2). β-GlcChol levels were also increased in the brains of *Gba1*$^{-/-}$/*Gba2*$^{+/-}$ medakas. The pattern was different for the other genotypes: in the brains of *Gba1*$^{+/+}$/*Gba2*$^{-/-}$, *Gba1*$^{+/-}$/*Gba2*$^{-/-}$, and *Gba1*$^{-/-}$/*Gba2*$^{-/-}$ medakas, β-GlcChol and β-GalChol levels were decreased. This is the pattern we observed in the brains of *Gba2*$^{-/-}$ mice. β-GalChol levels were also decreased in the brains of *Gba1*$^{-/-}$/*Gba2*$^{+/+}$ medakas, although this decrease was not statistically significant. In *Gba1*$^{-/-}$/*Gba2*$^{+/-}$, *Gba1*$^{+/+}$/*Gba2*$^{-/-}$, *Gba1*$^{+/-}$/*Gba2*$^{-/-}$, and *Gba1*$^{-/-}$/*Gba2*$^{-/-}$ medakas, GSX-2 and β-GlcSito levels were increased in the brains. These results suggest that GBA1 and GBA2 are both involved in the metabolism of brain sterylglycosides *in vivo*.

Cholesterol galactosylation is catalyzed by transgalactosylation of GBA1, GBA2, and GALC in vitro

To identify the enzyme responsible for β-GalChol formation, we experimentally down-regulated GBA1, GBA2, GALC (galactosylceramidase, galactocerebrosidase, EC 3.2.1.46), and CGT (UDP-galactose ceramide galactosyltransferase, EC 2.4.1.45) proteins by introducing specific targeting siRNA into β-GalChol- and GalCer-expressing H4 cells. GALC is a lysosomal enzyme responsible for degrading GalCer and galactosylsphingosine (GalSph). CGT is an enzyme responsible for synthesizing GalCer from ceramide and UDP-galactose (UDP-Gal). siRNA-mediated knockdown (KD) of GBA1, GBA2, GALC, or CGT reduced the level of each protein compared with that in control H4 cells; H4 cells received scrambled siRNA (Fig. 8*A*).

HILIC–ESI–MS/MS analysis of GalCer and β-GalChol showed that GBA1 KD or GBA2 KD reduced β-GalChol levels by about 50% (Fig. 8*B*). GBA1 KD or GBA2 KD did not alter GalCer levels. GALC KD resulted in the up-regulation of β-GalChol. We could not detect alteration of GalCer levels in H4 cells after GALC KD. Consistent with the results presented in Fig. 5, CGT KD reduced β-GalChol and GalCer levels, suggesting that β-GalChol expression depends on GalCer. These results suggest that GBA1, GBA2, and CGT are involved in β-GalChol formation and that GALC is involved in β-GalChol degradation.

Next, we examined whether glycolipids featuring terminal β-galactosyl residues, such as lactosylceramide, GA1, GM1, and GD1b, are suitable galactose donors for β-GalChol formation. We used HeLa cell mutants deficient in *UGCG*, a gene encoding UDP-glucose:ceramide glucosyltransferase (GlcCer synthase, EC 2.4.1.80). HeLa cell mutants deficient in *UGCG* (*UGCG*$^{-/-}$) express GalCer, but not GlcCer and GlcCer-derived glycolipids featuring terminal β-galactosyl residues (28). As expected, GlcCer and β-GlcChol concentrations were significantly reduced in *UGCG*$^{-/-}$ HeLa cells compared with WT HeLa cells (*UGCG*$^{+/+}$) (Fig. 8*C*). However, GalCer, β-GalChol, and β-GlcSito concentrations were not altered in *UGCG*$^{-/-}$ HeLa cells. The concentration of GSX-2 was below detection threshold in both cell lines. These results suggest that GalCer is one of the galactose donors needed for β-GalChol formation, whereas glycolipids featuring terminal β-galactosyl residues are not suitable galactose donors.

These findings prompted us to determine whether GBA1 and GBA2 could generate β-GalChol via transgalactosylation. We also examined whether GALC could also generate β-GalChol, even though GALC might be involved in β-GalChol degradation. Transgalactosylation *in vitro* was assessed using 25-NBD–cholesterol (NBD–chol) as a glycosyl acceptor. HPTLC and fluorescence scanning were used to detect any

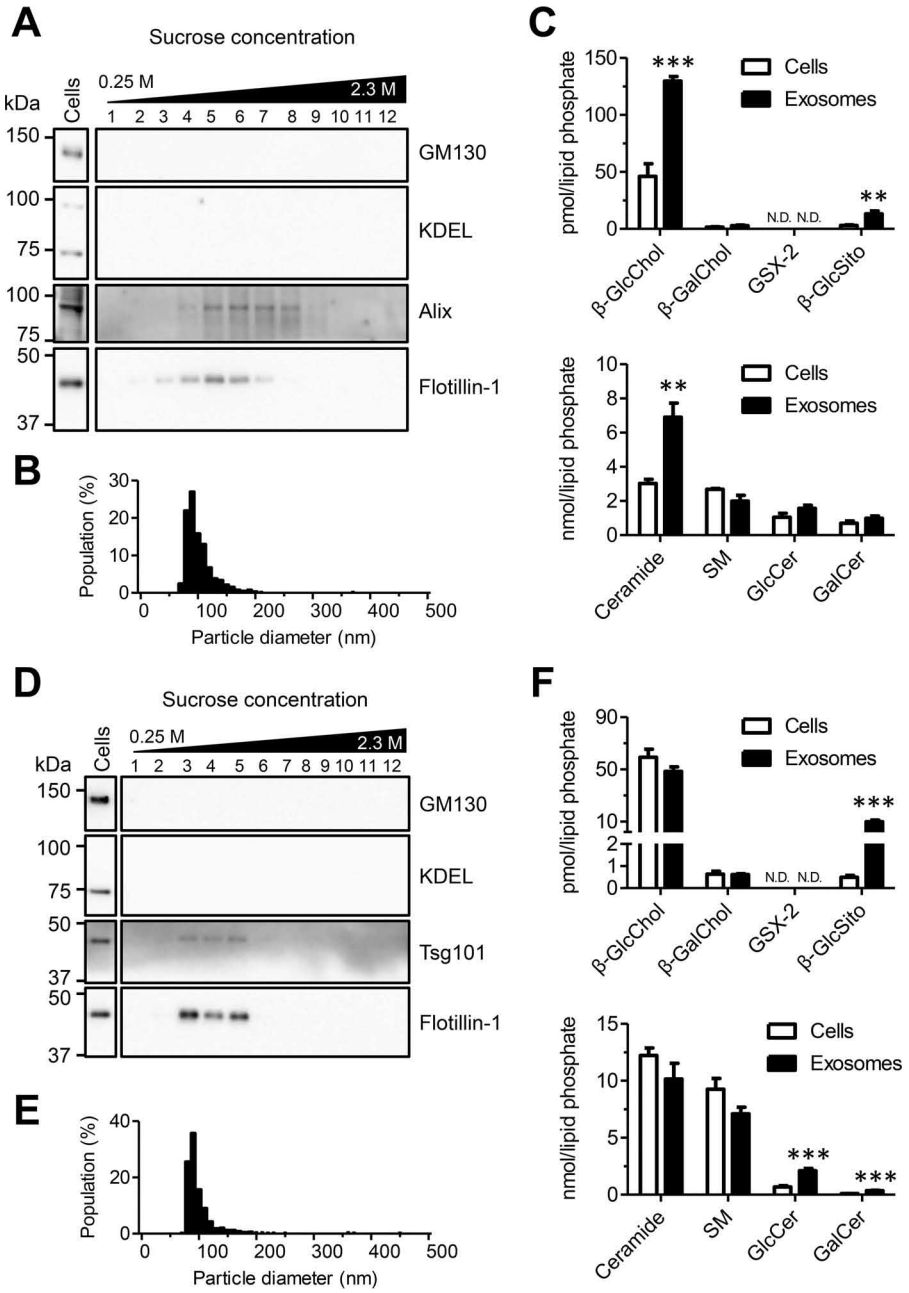

Figure 6. Secretion of sterylglycosides from H4 cells and mouse cortical neurons in association with exosomes. *A* and *D*, exosomes isolated from the culture supernatant of H4 cells (*A*) and mouse primary cortical neurons (*D*) were density-fractionated by sucrose gradient, and the fractions were analyzed by Western blotting to detect exosomal proteins (Alix, flotillin-1, and tsg101), GM130 and KDEL. The latter two are a marker protein for Golgi and an ER retention sequence, respectively. *B* and *E*, particle size distribution of the exosome fractions isolated from H4 cells (*B*) and mouse primary cortical neurons (*E*). *C* and *F*, concentrations of sterylglycosides, ceramide, SM, GlcCer, and GalCer in H4 cells (*C*), mouse primary cortical neurons (*F*), and isolated exosomes, as determined by LC–ESI–MS/MS. The quantitative values of ceramide or SM having various chain lengths of fatty acids (C16:0, C18:0, C20:0, C22:0, C24:0, and C24:1) are summarized. The quantitative values of GlcCer or GalCer having various chain lengths of fatty acids (C14:0, C16:0, C18:0, C20:0, C22:0, C22:1, C23:0, C23:1, C24:0, C24:1, C25:1, C26:0, and C26:1) are summarized. Data ($n = 4–5$) are means ± S.E. Differences were analyzed by unpaired *t* tests. **, $p < 0.01$; ***, $p < 0.001$; *N.D.*, not detected (below the detection threshold).

25-NBD–galactosyl-cholesterol (NBD–GalChol) formed. We used three enzyme sources: rGBA1, GBA2 (in the form of homogenates of GBA2-expressing HEK293T cells), and a recombinant human galactosylceramidase (rGALC). Each enzyme preparation was incubated with NBD–chol as the glycosyl acceptor and the following glycosyl donors: GlcCer (d18:1-C18:1); glucosylsphingosine (GlcSph); GalCer (d18:1-C12:0); GalSph; or UDP-Gal. Following incubation at optimal conditions for each enzyme, lipids were extracted and subjected to HPTLC.

Consistent with previous reports (2, 16), 25-NBD–glucosyl-cholesterol (NBD–GlcChol) was generated using 20 ng of rGBA1 protein and GlcCer (d18:1-C18:1) as glycosyl donor; NBD–GlcChol exhibited a similar R_f value as an authentic β-GlcChol standard. NBD–GlcChol formation was reduced by inhibiting GBA1 with CBE (Fig. 9*A*). Although NBD–GalChol

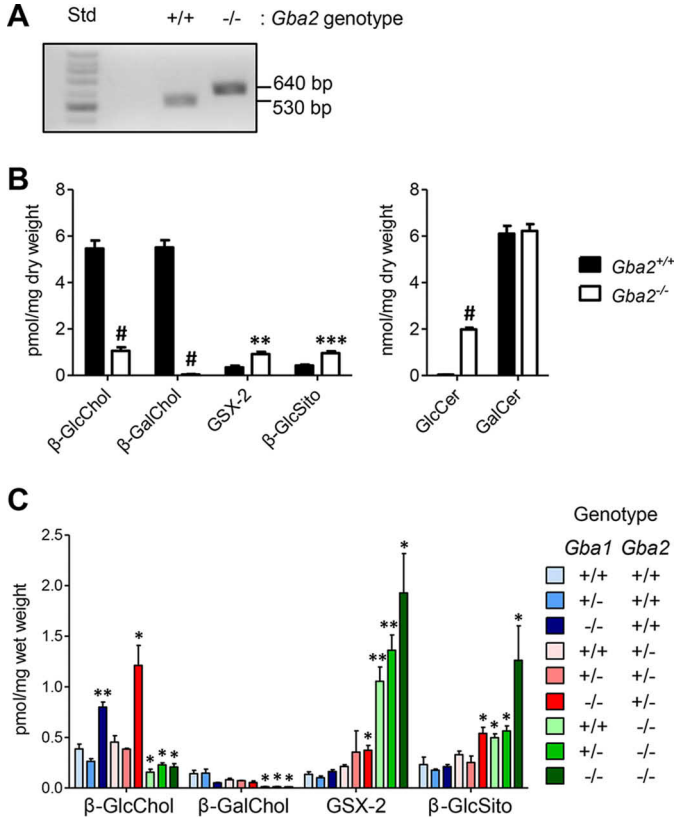

Figure 7. Effect of *Gba1* and/or *Gba2* knockout on sterylglycoside formation in brains of mice and medakas. *A* and *B*, effect of *Gba2* knockout on sterylglycoside formation in mouse brain. *A*, PCR genotyping of WT ($Gba2^{+/+}$) and $Gba2^{-/-}$ male mice genomic DNA. A 640-bp product was generated from the mutant allele, and a 530-bp product was produced from the WT allele. *B*, concentrations of sterylglycosides, GlcCer, and GalCer in brains of 10-week-old $Gba2^{+/+}$ and $Gba2^{-/-}$ male mice were analyzed by HILIC–ESI–MS/MS. Quantitative values of GlcCer or GalCer having various lengths of fatty acid chains (C16:0, C18:0, C20:0, C20:1, C22:0, C22:1, C23:0, C23:1, C24:0, C24:1, C25:0, C25:1, C26:0, and C26:1) are summarized. Data ($n = 4–5$) are means ± S.E. Differences were analyzed by unpaired *t* tests. **, $p < 0.01$; ***, $p < 0.001$; #, $p < 0.0001$. *C*, effect of *Gba1* and/or *Gba2* knockout on sterylglycoside formation in medaka brain. Concentrations of sterylglycosides in the 3.5-month-old medaka brains were analyzed by HILIC–ESI–MS/MS. These medakas were generated by crossing heterozygous mutants, which had a $Gba1^{+/-}/Gba2^{+/-}$ genotype. Data ($n = 3$) are means ± S.E. Differences were assessed by unpaired *t* tests. *, $p < 0.05$; **, $p < 0.01$ compared with WT ($Gba1^{+/+}/Gba2^{+/+}$).

formation was not detected using 20 ng of rGBA1 protein, NBD–GalChol was generated when we used more protein. Incubating 2 μg of the rGBA1 protein and GalCer (d18:1-C12:0) as glycosyl donor resulted in the formation of NBD–GalChol. The production of NBD–GalChol was reduced by CBE. In contrast, NBD–GalChol was not generated using rGBA1 and GalSph or UDP-Gal as glycosyl donors (Fig. 9*A*). The activity of rGBA1 toward NBD–GalChol formation was more than 1,000 times lower than that toward NBD–GlcChol formation. Consistent with a previous report (2), NBD–GlcChol was generated using 20 μg of protein in homogenates derived from GBA2-overexpressing HEK293T cells and GlcCer (d18:1-C18:1) as glycosyl donor. As expected, inhibition of GBA2 with *N*-(*n*-butyl)deoxygalactonojirimycin (NB-DGJ) reduced the amount of NBD–GlcChol formed (Fig. 9*B*). When using GalCer (d18:1-C12:0) as a glycosyl donor, more protein (200 μg of protein in HEK293T cell homogenates) was required to generate NBD–GalChol. NB-DGJ–mediated inhibition of GBA2 reduced the amount of NBD–GalChol formed (Fig. 9*B*). When GalSph or UDP-Gal was used as glycosyl donors in the presence of HEK293T cell homogenates, no NBD–GalChol was generated (Fig. 9*B*). The activity of GBA2 (in the homogenates) toward NBD–GalChol formation was more than 50 times lower than that toward NBD–GlcChol formation. As shown in the HPTLCs of Fig. 9*C*, NBD–GalChol was generated using rGALC and GalCer (d18:1-C12:0) as glycosyl donors; however, no NBD–GalChol was detected when GalSph or UDP-Gal was used as glycosyl donors.

We repeated the *in vitro* transgalactosylation activity assay using natural cholesterol as glycosyl acceptor and GalCer (d18:1-C12:0) as glycosyl donor. Formation of β-GalChol was assessed using HILIC–ESI–MS/MS (Fig. 9*D*). Again, β-GalChol was formed after incubating cholesterol for 2 h with rGBA1, homogenates from GBA2-overexpressing HEK293T cells, or rGALC. CBE and NB-DGJ, respectively, inhibited rGBA1- and GBA2-associated β-GalChol formation. Unexpectedly, a small amount of β-GalChol was formed in the absence of rGALC or without incubation (Fig. 9*D*, *right panel*). HILIC–ESI–MS/MS analysis confirmed that there was no β-GalChol contamination in any of the rGALC reaction mixtures (data not shown). This result indicates that trace amounts of β-GalChol could be formed by nonenzymatic reactions.

To transfer a galactose moiety from GalCer to cholesterol, hydrolysis of GalCer is necessary. Therefore, we analyzed the GalCer hydrolysis activity of rGBA1, of GBA2 in homogenates from GBA2-overexpressing HEK293T cells, and of rGALC using C_6-NBD–GalCer. HPTLC and fluorescence scanning was used to monitor the formation of the hydrolysis end product, C_6-NBD– ceramide (Fig. 9*E*). We also analyzed GlcCer hydrolysis activity using C_6-NBD–GlcCer. GlcCer hydrolysis occurred in the presence of rGBA1 and the HEK293T cell homogenates. GlcCer hydrolysis activity of rGBA1 and GBA2 (in homogenates) was inhibited by CBE and NB-DGJ, respectively. GalCer hydrolysis occurred in the presence of rGBA1, the HEK293T cell homogenates, and rGALC. The GalCer hydrolysis activity of rGBA1 and GBA2 (in homogenates) was inhibited by CBE and NB-DGJ, respectively. rGBA1 activity toward C_6-NBD–GalCer hydrolysis was ~200 times lower than that toward C_6-NBD–GlcCer hydrolysis. The GBA2 activity in homogenates toward C_6-NBD–GalCer hydrolysis was ~7 times lower than that toward C_6-NBD–GlcCer hydrolysis. These results suggest that GBA1, GBA2, and GALC have GalCer hydrolysis activity and transgalactosylation activity. These reactions transfer a galactose moiety from GalCer to cholesterol to form β-GalChol *in vitro*.

Sterylglycoside abnormalities in the brains of NPC disease model mice

NPC disease is a neurodegenerative lysosomal storage disease caused by loss–of–function mutations in either the *NPC1* or *NPC2* gene, genes that encode proteins essential for exporting cholesterol from lysosomes. Impairment of NPC1 or NPC2 leads to the accumulation of cholesterol in lysosomes; this accumulation is the primary defect in NPC disease (29, 30). β-GlcChol is remarkably elevated in the liver of $Npc1^{-/-}$ mice

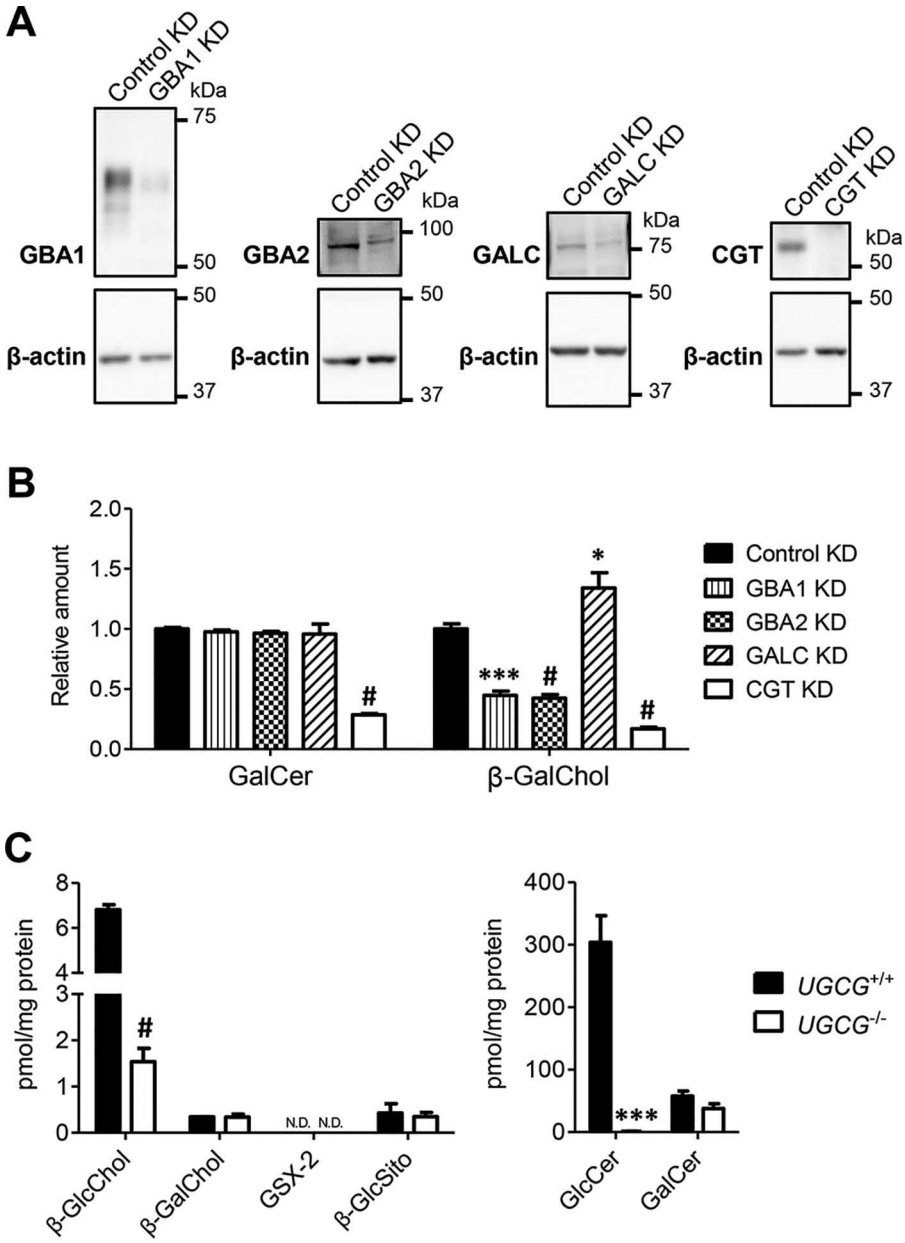

Figure 8. Sterylglycosides in cells manipulated in glycosphingolipid-metabolizing enzymes. *A* and *B*, effect of siRNA-mediated KD of GBA1, GBA2, GALC, or CGT on β-GalChol formation in H4 cells. GBA1, GBA2, GALC, and CGT proteins were down-regulated by introducing specific targeting siRNA into H4 cells. *A,* Western blot analysis of GBA1, GBA2, GALC, and CGT protein expression in H4 cells in which specific targeting siRNA was introduced. *B,* HILIC–ESI–MS/MS analysis of β-GalChol and GalCer concentration in H4 cells in which specific targeting siRNA was introduced. The quantitative values of GalCer having various lengths of fatty acid chains (C14:0, C16:0, C18:0, C20:0, C22:0, C22:1, C23:0, C23:1, C24:0, C24:1, C25:1, C26:0, and C26:1) are summarized. Data ($n = 3$–5) are means ± S.E. Differences were analyzed by unpaired *t* tests. *, $p < 0.05$; ***, $p < 0.001$; #, $p < 0.0001$. *C,* effect of *UGCG* knockout on sterylglycoside formation in HeLa cells. HILIC–ESI–MS/MS analyses of sterylglycosides, GlcCer, and GalCer concentration in HeLa-mCAT#8 cells ($UGCG^{+/+}$) and HeLa-mCAT#8 cell mutants deficient in *UGCG* ($UGCG^{-/-}$) are shown. Quantitative values of GlcCer or GalCer having various lengths of fatty acid chains (C14:0, C16:0, C18:0, C20:0, C20:1, C22:0, C22:1, C23:0, C23:1, C24:0, C24:1, C25:1, C26:0, and C26:1) are summarized. Data ($n = 3$–4) are means ± S.E. Differences were assessed by unpaired *t* tests. ***, $p < 0.001$; #, $p < 0.0001$; *N.D.*, not detected (below the detection threshold).

(NPC disease model), being 25 times higher compared with WT mice (2). β-GlcChol is also elevated in the plasma of patients with NPC disease (2). These findings prompted us to determine the concentration of sterylglycosides in the brains of $Npc1^{-/-}$ mice. The concentration of sterylglycosides, GlcCer, and GalCer was analyzed using HILIC–ESI–MS/MS (Fig. S2). Consistent with the up-regulation of β-GlcChol in the liver of $Npc1^{-/-}$ mice (2), the β-GlcChol level was elevated in the brains of $Npc1^{-/-}$ mice. Although the β-GalChol level was unchanged in the brains of $Npc1^{-/-}$ mice, levels of GSX-2 and β-GlcSito increased. As reported previously (31), we also found that GlcCer level was up-regulated and that GalCer level was down-regulated in the brains of $Npc1^{-/-}$ mice.

Discussion

Recently, we demonstrated aglycon heterogeneity in embryonic chicken brain— derived sterylglucosides by confirming the presence of β-GlcChol, GSX-2, and β-GlcSito (3). Here, we isolated two sterylglycoside fractions from 12-week-old rat brains. Structural analyses of sterylglycoside fractions GS1 and

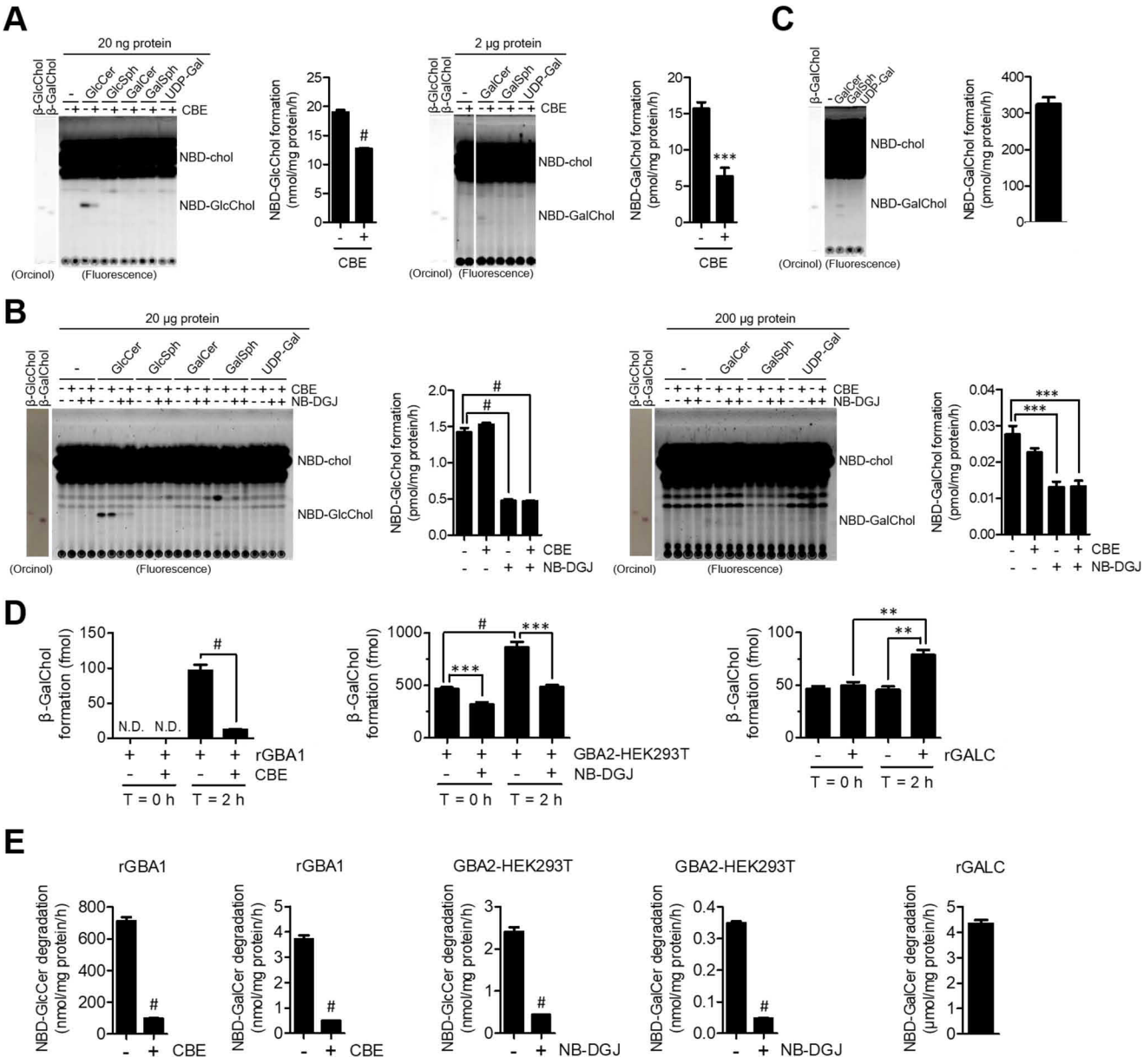

Figure 9. Assessment of *in vitro* transglycosylation activity of GBA1, GBA2, and GALC in the presence of various glycosyl donors. *A–C, in vitro* transglycosylation of NBD–GlcChol and NBD–GalChol by GBA1, GBA2, or GALC. rGBA1, homogenates derived from GBA2-overexpressing HEK293T cells or rGALC were incubated for 2 h with NBD– chol and GlcCer (d18:1-C18:1), GlcSph and GalCer (d18:1-C12:0), GalSph, or UDP-Gal as glycosyl donors. The samples were also incubated in the absence or presence of respective specific β-glucosidase inhibitors as follows: 0.5 mM CBE (for GBA1) and/or 0.3 mM NB-DGJ (for GBA2). Formation of NBD–GlcChol and NBD–GalChol was detected by HPTLC and fluorescence scanning. NBD–GlcChol and NBD–GalChol were identified by co-chromatography using authentic standards of β-GlcChol and β-GalChol, respectively. The authentic standards were visualized by spraying the HPTLC plates with orcinol reagent. *Bar graphs* show the concentrations of NBD–GlcChol formed in the presence of NBD– chol and GlcCer (d18:1-C18:1) and the concentrations of NBD–GalChol formed in the presence of NBD– chol and GalCer (d18:1-C12:0). Differences were analyzed by unpaired *t* tests; ***, $p < 0.001$; #, $p < 0.0001$. *A,* HPTLC analysis showing the quantification of NBD–GlcChol (*left image*) and NBD–GalChol (*right image*) formed in reactions comprising either 20 ng or 2 μg of rGBA1 protein as the enzyme source and the indicated glycosyl donors. Data presented as means ± S.E.; $n = 4$. *B,* HPTLC analysis showing the quantification of NBD–GlcChol (*left image*) and NBD–GalChol (right *image)* formed in reactions comprising either 20 or 200 μg of protein in homogenates derived from GBA2-overexpressing HEK293T cells as the enzyme source and the indicated glycosyl donors. Data are presented as means ± S.E.; $n = 4–6$. *C,* HPTLC analysis showing the quantification of NBD–GalChol formed in reactions comprising rGALC as the enzyme source and the indicated glycosyl donors. Data presented as means ± S.E.; $n = 4$. *D, in vitro* transgalactosylation of β-GalChol by GBA1, GBA2, and GALC. rGBA1, homogenates from GBA2-overexpressing HEK293T cells, or rGALC were incubated for 0 or 2 h with cholesterol in the presence of GalCer (d18:1-C12:0) as glycosyl donor and in the absence or presence of the respective specific β-glucosidase inhibitor: 0.5 mM CBE (for GBA1) or 0.3 mM NB-DGJ (for GBA2). Formation of β-GalChol was detected by HILIC–ESI–MS/MS. Differences ($n = 4–5$, means ± S.E.) were analyzed by unpaired *t* tests. **, $p < 0.01$; ***, $p < 0.001$; #, $p < 0.0001$; *N.D.,* not detected (below the detection threshold). *E, in vitro* GlcCer and GalCer hydrolysis activities of GBA1, GBA2, and GALC. rGBA1, homogenates from GBA2-overexpressing HEK293T cells, or rGALC was incubated for 30 min with C_6-NBD–GlcCer or C_6-NBD–GalCer and in the absence or presence of the respective specific β-glucosidase inhibitor: 0.5 mM CBE (for GBA1) or 0.3 mM NB-DGJ (for GBA2). HPTLC and fluorescence scanning were used to detect C_6-NBD– ceramide formation. Data presented as means ± S.E.; $n = 4–5$. Differences were analyzed by unpaired *t* tests; #, $p < 0.0001$.

GS2 revealed the presence of β-GlcChol and β-GalChol, respectively, representing the first report of β-GalChol in vertebrates. β-GalChol has previously been identified in *Borrelia burgdorferi* (32, 33), a bacterium causing Lyme disease. Lyme disease is the most common tick-borne disease in the Northern hemisphere. Additionally, the presence of GSX-2 and β-

GlcSito in adult rat brain, albeit at a 40 times lower abundance compared with β-GlcChol (data not shown), was confirmed. This low abundance of GSX-2 and β-GlcSito precluded further NMR spectroscopic analyses. As shown in Fig. 5, β-GalChol expression in the mouse brain relates to the presence of GalCer having long-chain fatty acid (>18 carbon atoms). GalCer with long-chain fatty acids (>18 carbon atoms) are enriched in myelin and are important for stabilizing myelin (34). Therefore, it is reasonable to suggest that β-GalChol could be a component of myelin. GalCer is quite abundant in the CNS, and its chromatographic behavior is very similar to that of β-GlcChol and β-GalChol. Because of this overlap with GalCer, it has been extremely difficult to isolate β-GlcChol and β-GalChol from brains for structural analysis, even when these are present. Our HILIC–ESI–MS/MS analysis revealed aglycon heterogeneity of sterylglucosides in rat, mouse, and medaka brain tissue, as well as in H4 cells, mouse primary cortical neurons, and HeLa cells. However, our HILIC–ESI–MS/MS analysis did not detect aglycon heterogeneity of sterylgalactoside, suggesting that cholesterol is the sole sterol aglycon of sterylgalactoside in vertebrates.

We showed that sterylglycosides are secreted from H4 cells and mouse primary cortical neurons in association with exosomes (Fig. 6). β-GlcChol has been demonstrated to be a neurotoxin *in vitro* (35), and β-GlcSito is a neurotoxin *in vitro* (36, 37) and *in vivo* (37–39). Thus, the secretion of β-GlcChol and/or β-GlcSito via exosomes might represent a cellular response to the buildup of toxic lipids in cells, providing a way to remove them from the cells. Exosomes have been hypothesized to participate in transferring pathogenic proteins between cells (40), such as β-amyloid peptide and α-synuclein, known to be associated with PD and MSA. Because mutations in *GBA1* appear to be involved in pathogenesis of PD and MSA (6, 7), it will be interesting to examine what role GBA1-metabolized sterylglycosides play in exosomal distribution of α-synuclein.

The levels of sterylglycosides were altered in the brains of GBA2-deficient mice and GBA1- and/or GBA2-deficient medakas. Consistent with a previous report (2), GBA1 seemed to be responsible for the degradation of β-GlcChol, and GBA2 for the formation of β-GlcChol. The level of β-GalChol was reduced in H4 cells in which specific targeting siRNA of GBA1 or GBA2 was introduced. β-GalChol was barely detected in the brains of GBA2-deficient mice and GBA2-deficient medakas. This suggests that GBA2 is the responsible enzyme for β-GalChol formation *in vivo*. Although it did not reach a statistically significant decline, β-GalChol levels were decreased in the brains of GBA1-deficient medakas, suggesting the involvement of GBA1 in β-GalChol formation. GBA2 seemed to be responsible for the degradation of GSX-2 and β-GlcSito. However, in the case of GBA2 deficiency, GBA1 seemed capable of degrading GSX-2 and β-GlcSito. Because GBA1 and GBA2 are localized to different cellular compartments, further experiments will be needed to determine the subcellular distribution of GSX-2 and β-GlcSito in order to understand the GBA1- and GBA2-mediated metabolic pathways.

It remains to be determined whether GSX-2 and β-GlcSito are *de novo*–synthesized in the brain and cultured cells, or whether they are derived from dietary intake or content in the culture media, respectively. The level of β-GlcSito did not change in $UGCG^{-/-}$ HeLa cells compared with WT HeLa cells. This suggests that GlcCer might not be the glucose donor for β-GlcSito formation in vertebrates. In plants, UDP-glucose:sterol glucosyltransferase (UDPG-SGTase, EC 2.4.1.173) is the enzyme responsible for β-GlcSito formation (1). Resolution of β-GlcSito formation in vertebrates remains stalled, as molecular cloning of the mammalian gene that shares homology with the known *UDPG-SGTase* gene has been unsuccessful.

Our *in vitro* enzyme assays revealed that GBA1, GBA2, and GALC exhibited β-gal activity and transgalactosylation activity. This reaction transfers a galactose residue from GalCer to cholesterol, leading to the formation of β-GalChol. This newly-detected activity against GalCer is significantly lower compared with their known activity against GlcCer. This enzyme's "promiscuity" of GBA1 and GBA2 has not been reported until now. Supporting our findings, it is known that D-galactose-configured deoxynojirimycins inhibit GBA1 and GBA2 (41). Also, in *Thermoanaerobacterium xylanolyticum*, a thermophilic anaerobic Gram-negative bacterium, not only does GBA2 have β-glucosidase activity, but it also has β-gal activity toward 4-nitrophenyl β-D-galactoside *in vitro* (42). Further structural analysis will be required to illuminate the differences between GalCer and GlcCer substrate recognition by GBA1 and GBA2.

GalCer is synthesized by CGT at the luminal side of the ER membrane (43) and is degraded by GALC at the luminal side of the lysosome (44). Burger *et al.* (45) showed transbilayer movement of GalCer in the membrane of cellular organelles, providing a rationale for GBA2-GalCer interaction at the cytosolic side of the ER membrane. In the lysosome, GalCer is located at the inner leaflet of the membrane and thus is readily accessed by GBA1 and GALC for β-GalChol synthesis. Although rGALC exhibited transgalactosylation activity to form β-GalChol *in vitro*, the level of β-GalChol increased in H4 cells that had specific siRNA targeting of GALC. Additionally, rGALC successfully released the aglycon from the isolated GS2 fraction predominantly containing β-GalChol. Together, this suggests that GALC might be responsible for β-GalChol degradation in cells. It would be of interest to determine the levels of β-GalChol in the Twitcher mouse, a naturally occurring model of Krabbe disease that lacks GALC protein. Although in this study we did not analyze the ability of CGT transgalactosylation *in vitro*, we found that UDP-Gal was not used as the donor for NBD–GalChol formation. Therefore, CGT might not be the enzyme responsible for β-GalChol formation.

We demonstrated in the brains of $Npc1^{-/-}$ mice several abnormalities of sterylglycosides, including up-regulation of β-GlcChol, GSX-2, and β-GlcSito. In NPC disease, excess cholesterol accumulates in lysosomes (30). GBA1 seems to promote β-GlcChol degradation under normal conditions; however, with excess cholesterol accumulation in lysosomes, GBA1 most likely synthesizes β-GlcChol (2). Therefore, the increased β-GlcChol in the brains of $Npc1^{-/-}$ mice might be synthesized by GBA1.

Marques *et al.* (31) showed that GBA2 activity is increased in the brains of $Npc1^{-/-}$ mice. This increased GBA2 activity might also cause up-regulation of β-GlcChol in the brains of $Npc1^{-/-}$ mice. In this study, our lipid analysis of GBA2-defi-

cient mouse brain revealed that GBA2 is responsible for degradation of GSX-2 and β-GlcSito. Although GBA2 activity is reportedly increased in the brains of *Npc1*$^{-/-}$ mice (31), we found that GSX-2 and β-GlcSito were elevated in the brains of *Npc1*$^{-/-}$ mice. It remains unclear where GSX-2 and β-GlcSito are distributed subcellularly and whether NPC1 exports GSX-2 and β-GlcSito from lysosomes. However, one explanation for the up-regulation of GSX-2 and β-GlcSito we detected in *Npc1*$^{-/-}$ mice is that export of GSX-2 and β-GlcSito from lysosomes is impaired.

Our results also have other significant implications for the treatment of GD, PD, MSA, cerebellar ataxia, and spastic paraplegia. It will be interesting to determine how these previously unrecognized functions of GBA1 and GBA2, demonstrated in this study, will aid our understanding of the role of GBA1 and GBA2 mutations in GD, PD, MSA, cerebellar ataxia, and spastic paraplegia.

Experimental procedures

Materials

β-GlcChol, GalCer from bovine brain, deuterated chloroform ($CDCl_3$, 99.96% D), 2,5-dihydroxybenzoic acid (DHB), cholesterol, and uridine 5′-diphosphogalactose disodium salt (UDP-galactose, UDP-Gal) were all purchased from Sigma-Aldrich. β-D-Glucopyranosyl-(1→1)-*N*-lauroyl-D-*erythro*-sphingosine (GlcCer [d18:1-C12:0]), β-D-galactopyranosyl-(1→1)-*N*-lauroyl-D-*erythro*-sphingosine (GalCer [d18:1-C12:0]), β-D-glucopyranosyl-(1→1)-*N*-stearoyl-D-*erythro*-sphingosine (GlcCer [d18:1-C18:0]), β-D-glucopyranosyl-(1→1)-*N*-oleoyl-D-*erythro*-sphingosine (GlcCer [d18:1-C18:1]), *N*-lauroyl-D-*erythro*-sphingosine (ceramide [d18:1-C12:0]), *N*-lauroyl-D-*erythro*-sphingosylphosphorylcholine (SM [d18:1-C12:0]), β-D-glucopyranosyl-(1→1)-D-*erythro*-sphingosine (GlcSph), β-D-galactopyranosyl-(1→1)-D-*erythro*-sphingosine (GalSph), 25-[*N*-[(7-nitro-2–1,3-benzoxadiazol-4-yl)methyl]amino]-27-norcholesterol (25-NBD– cholesterol, NBD– chol), and *N*-[6-[(7-nitro-2–1,3-benzoxadiazol-4-yl)amino]hexanoyl]-β-D-glucopyranosyl-(1→1)-sphingosine (C_6-NBD–GlcCer) were all purchased from Avanti Polar Lipids (Alabaster, AL). *N*-[6-[(7-nitro-2–1,3-benzoxadiazol-4-yl)amino]hexanoyl]-β-D-galactopyranosyl-(1→1)-sphingosine (C_6-NBD–GalCer) was purchased from Avanti Polar Lipids and Matreya LLC (State College, PA). *N*-Methyl-*N*-trifluoroacetamide (TMS) was from Acros Organics (Geel, Belgium). For LC–ESI–MS/MS, LC-MS– grade acetonitrile and methanol were purchased from Thermo Fisher Scientific (Waltham, MA); HPLC-grade chloroform and distilled water were purchased from Kanto Chemical Co., Inc. (Tokyo, Japan); ammonium formate was purchased from Sigma-Aldrich; and formic acid and ammonium acetate were purchased from FUJIFILM Wako (Osaka, Japan).

Cerezyme®, a recombinant human GBA1 (rGBA1) that is used in enzyme replacement therapy for GD (46), was purchased from Genzyme Japan (Tokyo, Japan). For *in vitro* enzyme assays, rGBA1 was dialyzed and deglycosylated according to reported methods (47). A recombinant human galactosylceramidase (GALC, galactocerebrosidase, EC 3.2.1.46) (rGALC) was purchased from R&D Systems, Inc. (Minneapolis, MN). CBE, an inhibitor of GBA1, was purchased from Enzo Life Sciences (Farmingdale, NY). NB-DGJ, an inhibitor of GBA2, was purchased from Toronto Research Chemicals, Inc. (North York, Ontario, Canada).

Animals and tissue collection

C57BL/6J mice were purchased from Japan SLC, Inc. (Hamamatsu, Japan). *Gba2*$^{-/-}$ mice (C57BL/6J-129S6/SvEv mixed background) were generated as described previously (9). Breeding pairs of *Gba2*$^{+/-}$ mice (C57BL/6J-129S6/SvEv mixed background) were a kind gift from Prof. Dr. Dagmar Wachten, University of Bonn (Bonn, Germany). *Gba2*$^{+/-}$ mice were back-crossed to the C57BL/6J background mice for 10 generations. *Gba2*$^{-/-}$ mice with the C57BL/6J background, along with WT littermates (*Gba2*$^{+/+}$), were generated by crossing the back-crossed *Gba2*$^{+/-}$ males and females in-house. Offspring mice were genotyped by PCR using genomic DNA as described previously (9). These mice were housed in the RIKEN Center for Brain Science animal housing facilities under a 12-h light/12-h dark on/off cycle and at a constant room temperature of 23 ± 2 °C. The mice had free access to water and standard mouse chow (CRF-1, Oriental Yeast Co., Ltd., Tokyo, Japan). Experimental protocols for the animal experiments were approved by RIKEN's Wako Animal Experiments Committee.

For collection and preparation of tissue for biochemical analyses, postnatal mice were deeply anesthetized and perfused with PBS. Whole brains were surgically removed, directly snap-frozen in liquid nitrogen, and stored at −80 °C until lyophilized. After lyophilization, samples were stored at −80 °C until further use. For tissue collection from embryonic mice, we used embryos of pregnant C57BL/6J mice that were purchased from Japan SLC, Inc. Pregnant mice were deeply anesthetized, and the uterus together with the embryos were transferred to ice-cold PBS. The uterus was cut, and the embryonic sacs were removed to release embryos into the PBS. The released embryos were transferred to ice-cold Hanks' balanced salt solution (Nacalai Tesque, Inc., Kyoto, Japan). Whole brains were surgically removed, directly snap-frozen in liquid nitrogen, and stored at −80 °C until lyophilized. After lyophilization, samples were stored at −80 °C until further use. From P10 to postnatal week 10, male mice were used for tissue collection. From E12 to P2, sex of the mice was not discriminated.

Npc1$^{-/-}$ mice (*Npc1*^{nih}, BALB/c background), along with WT littermates (*Npc1*$^{+/+}$), were generated as described previously (2). These mice (±3 weeks old) received the rodent AM-II diet (Arie Blok Diervoeders, Woerden, The Netherlands). The mice were housed at the Institute Animal Core Facility in a temperature- and humidity-controlled room with a 12-h light/dark on/off cycle, and they were given free access to food and water *ad libitum*. Offspring were genotyped by PCR using genomic DNA, as described previously (48). Experimental protocols for these animal experiments were approved by the Institutional Animal Welfare Committee of the Academic Medical Centre Amsterdam in the Netherlands. For collection and preparation of tissue for biochemical analyses, male mice were first anesthetized with an intramuscular injection of Hypnorm® (comprising 0.315 mg/ml phenyl citrate and 10 mg/ml fluani-

sone; VetaPharma Ltd., Leeds, UK) and Dormicum (5 mg/ml midazolam; Teva Pharmaceutical Industries Ltd., Parsippany, NJ). The dose was adjusted according to their weight (80 μl/10 g bodyweight). These mice were euthanized by cervical dislocation. Whole brains were surgically removed, rinsed with PBS, directly snap-frozen in liquid nitrogen, and stored at −80 °C until lyophilized. After lyophilization, samples were stored at −80 °C until further use.

Generation of Gba1$^{+/-}$/Gba2$^{+/-}$ medakas and preparation of medaka brains

Medakas (*O. latipes*) are an ideal vertebrate animal model for our purposes, because deletion of GBA1 in fish does not cause perinatal death (49–51). Previously, Uemura *et al.* (49) generated *Gba1* nonsense mutant (*Gba1*$^{-/-}$) medaka. In contrast to the perinatal death in humans and mice lacking GBA1 activity, *Gba1*$^{-/-}$ medakas survived for months, enabling biochemical and behavioral analyses of adult stage.

The ethics statement and maintenance of medakas were described previously (49). Medaka experiments were approved by the Animal Experiments Committee of Kyoto University and were conducted in accordance with Japanese national guidelines. Medakas were maintained in an aquaculture system with recirculating water at 27 °C in a 14-h light/10-h dark cycle.

Medakas of the Kyoto-cab strain, a substrain of Cab, were used. The details of *Gba1*$^{-/-}$ medakas were reported previously (49). GBA2-deficient medakas were generated by using clustered, regularly-interspaced short palindromic repeats (CRISPR)/CRISPR-associated9 (Cas9) system, as reported previously (52). Briefly, the cDNA sequence of medaka GBA2 was determined by RT-PCR and rapid amplification of cDNA ends.

The medaka *GBA2* gene consists of 18 exons that encode 858 amino acids. The crRNAs were generated using the CRISPR design tool (RRID:SCR_018159), and the following crRNA was used: 5′-GGAGGGCAAAGCACTGTCGGGGG-3′. The crRNAs and tracrRNA were constructed by Fasmac Co. (Kanagawa, Japan). The Cas9 RNA was synthesized from a pCS2+hSpCas9 vector (catalogue no. 51815, Addgene, Watertown, MA) using a mMessage mMachine SP6 kit (Thermo Fisher Scientific). The RNA mixture was injected into single-cell–stage embryos. The injected founders (F_0) were raised to sexual maturity and back-crossed with WT medakas for generating F_1s. The *GBA2* gene of the F_1s was sequenced, and the novel GBA2-deficient (*Gba2*$^{+/-}$) medakas with 21 bases deleted and two bases inserted into exon 5 were obtained.[3] These deletions and insertions resulted in a frameshift mutation, leading to a deficiency in GBA2 protein expression and enzymatic activity of GBA2 in the brain. Off-target candidates were searched using the Medaka pattern match tool (RRID:SCR_018157). No alterations were found in three off-target candidates located on exons.

Gba2$^{+/-}$ medakas were back-crossed with WT medakas at least five times, and then crossed with GBA1-deficient medakas to create *Gba1*$^{+/-}$/*Gba2*$^{+/-}$ medakas. Medaka brains collected by surgery were directly snap-frozen in liquid nitrogen and then stored at −80 °C until use.

Cell cultures

Human neuroglioma H4 cells (HTB-148^{TM}) were purchased from the ATCC (Manassas, VA). They were cultured in Dulbecco's modified Eagle's medium (DMEM, FUJIFILM Wako) supplemented with 10% (v/v) fetal bovine serum (FBS). Cultures were maintained in a 5% CO_2 atmosphere at 37 °C. HeLa-mCAT#8 cells, a parent cell line, and HeLa-mCAT#8 cell mutants deficient in *UGCG* (28) were a generous gift from Dr. Toshiyuki Yamaji of the National Institute of Infectious Diseases (Tokyo, Japan). *UGCG* is a gene that encodes UDP-glucose:ceramide glucosyltransferase (GlcCer synthase) (53). These cells were also cultured in DMEM supplemented with 10% FBS and were maintained in a 5% CO_2 atmosphere at 37 °C. Stable human GBA2-expressing human embryonic kidney (HEK) 293T cells were generated as described previously (54). HEK293T cells were cultured in DMEM (Sigma-Aldrich) supplemented with 10% (v/v) FBS, 200 μg/ml penicillin/streptomycin, and 1% (v/v) GlutaMAX and were maintained in a 7% CO_2 atmosphere at 37 °C. For enzyme assays, cell pellets of the stable human GBA2-expressing HEK293T cells were obtained using standard methods. The cell pellets were suspended in McIlvaine buffer (0.1 M citric acid and 0.2 M Na_2HPO_4 (pH 5.8)) containing 0.1% (w/v) bovine serum albumin (BSA) and were then sonicated.

For primary neuron cultures, we used embryos of pregnant Slc:ICR mice that were purchased from Japan SLC, Inc. These cultures were prepared from the cerebral cortices of Slc:ICR mouse brains on embryonic day 14, according to the methods of Yuyama *et al.* (26), with some modifications. Briefly, neurons for culturing were obtained from the isolated cerebral cortices using a neuron dissociation solution (FUJIFILM Wako). The dissociated cells were plated onto poly-L-ornithine–coated dishes at a density of 3.16×10^5 cells/cm^2 and cultured in Neurobasal^{TM} medium (Thermo Fisher Scientific) supplemented with GlutaMAX^{TM} supplement (Thermo Fisher Scientific), 1 mM sodium pyruvate, 100 units/ml penicillin, 100 μg/ml streptomycin, and B-27^{TM} supplement (Thermo Fisher Scientific). One day after plating, cytosine β-D-arabinofuranoside (Sigma-Aldrich) was added to the culture at a final concentration of 10 μM to inhibit the proliferation of dividing non-neuronal cells. Three and 6 days after plating, half of the culture supernatant from each dish was collected and replaced with fresh medium. Nine days after plating, all the culture supernatants were collected. The collected culture supernatants were combined and then used for exosome isolation.

Enrichment of sterylglycosides

Frozen brains of 12-week-old male Wistar rats were purchased from Japan Lamb Ltd. (Hiroshima, Japan). Total lipids were extracted from lyophilized brains (100 brains, 45 g dry weight) using 400 ml of chloroform and methanol (C/M at 2:1, v/v) twice and 200 ml of C/M (1:1, v/v). After evaporation, the combined extracts were hydrolyzed for 3 h at room temperature in C/M (2:1, v/v, 240 ml) containing 0.1 M KOH. The reaction mixture was subjected to Folch's partition (55), and the lower phase was evaporated to dryness. The resulting lipid film was resuspended in chloroform (100 ml) and applied to a col-

umn of Silica Gel 60 (Kanto Chemical Co., Inc.) equilibrated with chloroform. Glycolipids, including sterylglycosides, were eluted using a stepwise gradient, starting with pure chloroform (400 ml) and then with C/M (98:2, v/v, 400 ml), C/M (95:5, v/v, 400 ml), C/M (9:1, v/v, 600 ml), and C/M (8:2, v/v, 600 ml). The fractions eluted with C/M (9:1, v/v) containing sterylglycosides alongside hexosylceramide were pooled and evaporated until dry. The lipid film was resuspended in ~150 ml of a methanol/water mixture (M/W at 95:5, v/v), and the soluble fraction (~120 ml) was subjected to RP column chromatography over Silica Gel 120 (RP-18; Kanto Chemical Co., Inc.), which was equilibrated with M/W (95:5, v/v). Elution was facilitated by using a stepwise gradient of M/W (95:5, v/v, 300 ml) and methanol (200 ml). The presence of sterylglycosides was evaluated using HPTLC, and positive fractions were pooled and dried.

Isolation of sterylglycosides

The enriched sterylglycoside fraction was further purified by normal-phase HPLC. The lipid film was resuspended in a small volume of mobile phase A (C/M at 98:2, v/v), applied to a PEGASIL Silica SP100–3 column (4.6 mm inner diameter × 250 mm, particle size, 3 μm; Senshu Scientific Co., Ltd., Tokyo, Japan), and eluted with the following gradients of mobile phase B (C/M/W at 80:20:0.2, v/v/v): 10 min, 0%; 60 min, 0–100% linear gradient; and 10 min, 100% (washing step). The flow rate was kept constant at 0.5 ml/min, and the column was maintained at room temperature. The eluent was collected once per min. The presence of sterylglycosides was evaluated using HPTLC, and positive fractions were pooled and dried.

The further enriched sterylglycosides fraction was dissolved in a small volume of C/M (2:1, v/v), applied to a HPTLC plate (Silica Gel 60; Merck Millipore, Darmstadt, Germany), impregnated with 1% boric acid, and developed with hexane/isopropyl alcohol/C/M/W (25:35:65:25:3, v/v/v/v/v). Lipids were stained with primuline reagent (0.002% primuline, 80% acetone) and visualized with long-wave UV. The bands co-migrating with standard β-GlcChol and β-GalChol were each collected, extracted by Folch's partition, and designated as GS1 and GS2, respectively. The organic layer containing sterylglycosides was collected and dried under a stream of nitrogen gas (N_2).

Enzymatic deglycosylation of sterylglucosides

Aglycon release from the GS1 fraction was performed as described previously (3). Aglycon release from the GS2 fraction was performed as described previously (56), with minor modifications as follows. A portion of the GS2 fraction was dissolved in C/M (2:1, v/v) and taken to dryness. This portion was then suspended in 10 μl of 0.1% Triton X-100 followed by sonication. Next, 0.4 mg of oleic acid (Sigma-Aldrich) dissolved in C/M (2:1, v/v) was taken to dryness and then dispersed by sonication in 40 μl of 70 mg/ml sodium taurocholate containing 0.1% Triton X-100. To release aglycon from the GS2 fraction, we made a reaction mixture in a total volume of 100 μl, which contained 10 μl of the dispersed oleic acid, 10 μl of the dispersed GS2 fraction, and 860 ng of rGALC in 50 μl of McIlvaine buffer (pH 4.1). The reaction mixture was incubated at 37 °C for 20 h. The reaction was terminated by addition of 2 ml of C/M (2:1, v/v) and 400 μl of water (adjusted to a total volume of 500 μl, including the reaction mixture) to facilitate lipid extraction by Folch's partition. The organic layer was separated and dried. The sterol fraction was purified by HPTLC on Silica Gel 60 using hexane/diethyl ether/acetic acid (80:20:1, v/v/v) as an eluent. Lipids were stained by primuline reagent and visualized by long-wave UV. The band that co-migrated with standard cholesterol (FUJIFILM Wako) was collected and extracted by Folch's partition. The organic layer containing the released aglycons was separated and dried under a stream of N_2.

GC/MS analysis

The lipid containing released aglycons was suspended in 25 μl of TMS and was incubated at room temperature for 30 min. The resulting trimethysilylated material was subjected to GC/MS analysis on a GC system 7890A (Agilent Technologies Inc., Santa Clara, CA) attached to a mass spectrometer, JMS-T100GCV AccuTOF GCv 4G (JEOL Ltd., Tokyo, Japan). An HP-5ms capillary column (30 m × 0.25 mm, film thickness of 0.25 μm; Agilent Technologies Inc.) was interfaced with the GC system. We employed the following temperature gradient: from 130 to 250 °C at a heating rate of 20 °C/min, and from 250 to 300 °C at a heating rate of 5 °C/min.

MALDI-TOF/TOF analysis

The GS1 fraction, GS2 fraction, and authentic standards of β-GlcChol and β-GalChol were each dissolved in C/M (2:1, v/v) at a concentration of ~0.5 μg/μl, then mixed with MALDI matrix A (10 μg/μl of DHB in C/M, 1:1, v/v) and B (1 μg/μl LiCl in methanol) at a ratio of 1:1:1 (v/v/v). One μl of the resulting mixture was spotted onto an MTP 384 target plate of polished steel BC (Bruker, Billerica, MA) and dried. The samples were analyzed with an autoflex speed TOF/TOF (Bruker) equipped with the TOF/TOF option. A Smartbeam II Nd:YAG laser pulse of 355 nm was operated at 2 kHz. For product–ion mass spectrum acquisition, argon collision gas was introduced. The collision energy of 6 keV was used to induce high-energy CID.

LC–ESI–MS/MS analysis

The LC–ESI–MS/MS analysis was performed on an LC system Nexera X2 (SHIMADZU, Kyoto, Japan) attached to a triple-quadrupole linear ion trap mass spectrometer, QTRAP4500 (SCIEX, Tokyo, Japan). The LC–ESI–MS/MS datasets were analyzed with MultiQuant™ (version 2.1) and Analyst software (SCIEX). Target lipids were monitored in MRM mode using specific precursor–product ion pairs, as detailed in Table S2.

GlcCer, GalCer, and sterylglycosides were analyzed, as reported previously (3, 18), by HILIC–ESI–MS/MS with minor modifications. In brief, the lipid extracts were dissolved in C/M (2:1, v/v) and diluted 10-fold with mobile phase A (acetonitrile/methanol/formic acid, 97:2:1, v/v/v, with 5 mM ammonium formate). Aliquots (10 μl) were applied to an Atlantis silica HILIC column (2.1 mm inner diameter × 150 mm, particle size, 3 μm; Waters) maintained at 40 °C. Samples were eluted at a flow rate of 0.05 ml/min using the following gradient of mobile phase B (methanol/water/formic acid, 89:9:1, v/v/v, with 20 mM ammonium formate): 3.3 min, 0%, 23.4 min, 0–35% linear gradient; 1.3 min, 35–70% linear gradient, 0.05–0.15 ml/min linear gra-

dient flow rate; 8 min, 70% (washing step); 29 min, 0%, flow rate increased to 0.2 ml/min (equilibration); 2 min, 0%, flow rate decreased to 0.05 ml/min. The mass spectrometer was set to positive ion mode (ion spray voltage, 5500 V; curtain gas pressure, 30 p.s.i.; nebulizer gas pressure, 90 p.s.i.; heating gas pressure, 30 p.s.i.; temperature, 100 °C) using MRM detection for a targeted analysis. Ionization efficiency of GlcCer and GalCer were similar under the employed conditions.

Ceramide, SM, and sterylglycosides were analyzed by RPLC–ESI–MS/MS. The lipid extracts were dissolved in C/M (2:1, v/v) and were diluted 10-fold with mobile phase B (M/W 85:15, v/v, with 5 mM ammonium acetate). The diluted lipid extracts were applied onto an RP column (Luna C18(2) column: 2 mm inner diameter × 250 mm, particle size, 3 μm; Phenomenex, Torrance, CA) maintained at 36 °C and at a flow rate of 0.15 ml/min. The samples were then eluted with the following gradients of mobile phase A (methanol pure, with 5 mM ammonium acetate): 2 min, 0%; 13 min, 0–100% linear gradient; 40 min, 100% (washing step); 15 min 0% (equilibration). For ceramide and SM analysis, the mass spectrometer was set to positive ion mode (ion spray voltage, 5,500 V; curtain gas pressure, 40 p.s.i.; nebulizer gas pressure, 70 p.s.i.; heating gas pressure, 80 p.s.i.; temperature, 600 °C) using MRM detection for targeted analysis. For sterylglycoside analysis, the mass spectrometer was set to positive ion mode (ion spray voltage, 5,500 V; curtain gas pressure, 20 p.s.i.; nebulizer gas pressure, 80 p.s.i.; heating gas pressure, 40 p.s.i.; temperature, 100 °C), using either MRM detection for targeted analysis or neutral-loss scan for untargeted analysis. The parameters for the latter were as follows: 197 Da, calculated as loss of hexose and NH_3; scan speed, 200 Da/s; collision energy, 15 eV.

NMR spectroscopy

Highly-purified sterylglycoside fractions and authentic standards were dissolved in $CDCl_3$ containing tetramethylsilane as an internal chemical shift reference. One-dimensional ^1H NMR and two-dimensional double-quantum filtered correlation spectroscopy, homonuclear Hartmann-Hahn (HOHAHA) spectra, and ^1H–^{13}C multiplicity–edited HSQC spectra were recorded on an Avance-500 spectrometer (Bruker BioSpin, Yokohama, Japan) equipped with a triple-resonance (TXI) cryogenic probe and an Avance-600 spectrometer with a TXI probe. Probe temperature was set at 25 °C. The NMR data were processed with TopSpin software (version 2.1; Bruker BioSpin), and the spectra were displayed using TopSpin Plot Editor (version 2.1; Bruker BioSpin).

Chemical synthesis of 1-O-cholesteryl-β-D-galactopyranoside

All solvents and reagents were purchased from commercial suppliers as reagent grade and were used as is. Reactions with anhydrous solvents (Kanto Chemical Co., Inc.) were performed under an argon atmosphere. Flash column chromatography was performed with Silica Gel 60 N (40–100 mesh, Kanto Chemical Co., Inc.) and the indicated solvent systems. Analytical TLC was performed on Silica Gel 60 F256 plates (Merck Millipore). Mass spectra were recorded on an AccuTOF JMS-T700LCK (JEOL) using ESI. NMR spectra were obtained on an ECX-500 spectrometer (JEOL) in the indicated solvent system at 25 °C using residual nondeuterated solvent signals as chemical shift references.

Cholesteryl 2,3,4,6,-tetra-*O*-acetyl-β-D-galactopyranoside was synthesized as follows. 2,3,4,6-Tetra-*O*-acetyl-α-D-galactopyranosyl 2,2,2-trichloroacetimidate (2.0 g, 4.06 mmol, 1.2 Eq) and cholesterol (Chol) (1.3 g, 3.37 mmol, 1.0 Eq) were dissolved in anhydrous dichloromethane (20 ml) at −40 °C. After 10 min, the coupling was initiated by addition of TMS (20 μl, 24.6 mg, 0.11 mmol) and stirred for 2 h at −40 °C. The reaction was quenched with triethylamine (3 ml); the organic layer was increased with dichloromethane (20 ml); and the resulting mixture was extracted twice against water (20 ml) and once against brine (20 ml). The organic layer was dried over Na_2SO_4, concentrated under reduced pressure, and subjected to flash chromatography (hexane/ethyl acetate = 4:1) to yield cholesteryl 2,3,4,6,-tetra-*O*-acetyl-β-D-galactopyranoside (1.45 g, 2.02 mmol, 60%) as a white solid. TLC, hexane/ethyl acetate = 5:1; ^1H NMR (500 MHz, $CDCl_3$): δ 5.37 (d, 1H, J = 3.4, Gal), 5.36 (m, 1H, J = 5.2, Chol DB), 5.18 (dd, 1H, J = 10.3, J = 8.0, Gal), 5.02 (dd, 1H, J = 10.3, J = 3.4, Gal), 4.54 (d, 1H, J = 8.0, Gal H-1), 4.18 (dd, 1H, J = 11.2, J = 6.6, Gal), 4.12 (dd, 1H, J = 14.3, J = 6.9, Gal), 3.88 (dd, 1H, J = 6.9, J = 6.3, Gal), 3.48 (m, 1H, Chol H-3), 2.14 (s, 3H, Ac CH_3), 2.06 (s, 3H, Ac CH_3), 2.04 (s, 3H, Ac CH_3), 1.98 (s, 3H, Ac CH_3), 2.27–1.80 (n.r., 8H, Chol), 0.99 (s, 3H, Chol CH_3), 0.91 (d, 3H, J = 6.3, Chol CH_3), 0.87 (d, 3H, J = 2.3, Chol CH_3), 0.85 (d, 3H, J = 2.3, Chol CH_3), 1.68–0.85 (n.r., 20H, Chol), 0.67 (s, 3H, Chol CH_3) ppm; ^{13}C NMR (125 MHz, $CDCl_3$): δ 170.8, 170.7, 170.6, 169.8 (4C, Ac CO), 140.7 (1C, Chol DB), 122.5 (1C, Chol DB), 100.6 (1C, Gal C-1), 80.7 (1C, Chol C-3), 71.4, 70.9, 69.4, 67.4 (4C, Gal CH), 61.7 (1C, Gal CH_2), 57.1, 56.5, 50.5, 42.7, 40.1, 39.9, 39.3, 37.5, 37.1, 36.5, 36.1, 32.3, 32.2, 29.9, 28.6, 28.4, 24.6, 24.2, 23.2 (18C, Chol), 22.9 (2C, Chol CH_3), 21.4 (1C, Chol), 21.2, 21, 21 (4C, Ac CH_3), 19.7 (1C, Chol CH_3), 19.1 (1C, Chol CH_3), 12.2 (1C, Chol CH_3) ppm.

β-GalChol was synthesized as follows. Cholesteryl 2,3,4,6,-tetra-*O*-acetyl-β-D-galactopyranoside (0.7 g, 0.98 mmol, 1.0 Eq) was dissolved in anhydrous dichloromethane (10 ml) and treated with freshly-prepared sodium methoxide solution (10 ml of anhydrous methanol with 10 mg of sodium). The suspension was stirred for 2 h at room temperature, quenched with acetic acid (52 μl, 50 mg), and evaporated to dryness. The resulting solid was suspended in hot ethanol and filtered, and the filter cake was further rinsed with hot ethanol. The filter cake was dried under high vacuum to give β-GalChol (300 mg, 0.547 mmol, 56%) as a white solid.

The filtrate was evaporated and subjected to flash chromatography (gradient of chloroform/methanol = 20:1 to 10:1, v/v). TLC, chloroform/methanol = 9:1 (v/v), R_f = 0.56; ^1H NMR (500 MHz, $CDCl_3$/methanol = 1:3, v/v): δ 5.34 (d, 1H, J = 5.2, Chol DB), 4.33 (d, 1H, J = 8.0, Gal H-1), 3.88 (m, 1H, Gal), 3.79–3.72 (n.r., 2H, Gal), 3.61–3.56 (n.r., 2H, Gal, Chol H-3), 3.50–3.46 (n.r., 2H, Gal), 2.38 (m, 1H, Chol), 2.25 (m, 1H, Chol), 2.01–1.78 (n.r., 5H, Chol), 1.73–0.90 (n.r., 21H, Chol), 0.99 (s, 3H, Chol CH_3), 0.90 (d, 3H, J = 6.3, Chol CH_3), 0.85 (d, 3H, J = 6.9, Chol CH_3), 0.84 (d, 3H, J = 6.3, Chol CH_3), 0.67 (s, 3H, Chol CH_3) ppm; ^{13}C NMR (125 MHz, $CDCl_3$: methanol = 1:3): δ 141.5 (1C, Chol DB), 123.1 (1C, Chol DB), 102.6 (1C, Gal C-1), 79.9 (1C, Chol C-3), 75.7, 74.6, 72.5, 69.9 (4C, Gal CH), 62.4 (1C,

Gal CH_2), 57.8, 57.2, 51.3, 43.4, 40.8, 40.6, 39.7, 38.3, 37.8, 37.2, 36.8, 33, 30.7, 30.6, 29.3, 29, 25.3, 24.9 (18C, Chol), 23.7, 23.5 (2C, Chol CH_3), 22.1 (1C, Chol), 20.3 (1C, Chol CH_3), 19.7 (1C, Chol CH_3), 12.8 (1C, Chol CH_3) ppm; ESI-MS calculated for $C_{33}H_{56}O_6$ $[M + Na]^+$: *m/z* 571.397, and found: 571.36.

Quantification of lipids in animal tissue

Lyophilized tissue and frozen tissue were homogenized, and total lipids were extracted with C/M (2:1, v/v, 5 ml) mixture added to 5 pmol/mg lyophilized tissue or to 1 pmol/mg frozen tissue of GlcCer (d18:1-C12:0), and β-GlcChol-d_7 (3) served as internal standard. Extracts were dried under a flow of N_2 and hydrolyzed for 2–3 h at room temperature in C/M (2:1, v/v, 2–3 ml) containing 0.1 M KOH. After neutralization with 7.5 μl of glacial acetic acid, the reaction mixture was subjected to Folch's partition, and the lower phase was dried under a flow of N_2. The resulting lipid film was suspended in C/M (2:1, v/v) at a concentration of ~40 μg of lyophilized tissue/μl or ~100 μg of frozen tissue/μl, and diluted 10-fold with mobile phase A for HILIC–ESI–MS/MS analysis. Aliquots (10 μl) were subjected to HILIC–ESI–MS/MS analysis. The resulting peak areas were integrated and quantified relative to the associated internal standard.

Quantification of lipids in cultured cells and exosomes

Frozen cells and frozen exosomes were resuspended in 250 μl of water and sonicated. Protein concentration was determined by a Pierce™ BCA protein assay kit (Thermo Fisher Scientific). Water was added to the homogenate up to 400 μl, and then 1.5 ml of C/M (1:2, v/v), ~10 pmol of GlcCer (d18:1-C12:0), β-GlcChol-d_7, ceramide (d18:0-C12:0), and SM (d18:1-C12:0), each as internal standards, were added. The sample was sonicated and centrifuged at 3,000 rpm for 10 min at room temperature, and the supernatant was collected. A volume (1.9 ml) of C/M/W (1:2:0.8, v/v/v) was added to the remaining pellet, and then the sample was sonicated and centrifuged as described above. The supernatant was collected and combined with the first supernatant.

Next, lipids were extracted according to the method of Bligh and Dyer (57) by adding 1 ml of chloroform and water each; the lower phase was taken to dryness under a flow of N_2. For glycolipid analysis, a portion of the sample was hydrolyzed with KOH as described above. The resulting lipid film was suspended in C/M (2:1, v/v) at a concentration of ~150 μg of protein/μl and diluted 10-fold with mobile phase B for RPLC–ESI–MS/MS analysis or mobile phase A for HILIC–ESI–MS/MS analysis. Aliquots (10 μl) were subjected to RPLC–ESI–MS/MS or HILIC–ESI–MS/MS analysis, respectively. The resulting peak areas were integrated and quantified relative to the associated internal standard. For comparing lipid concentrations of exosomes and their cells of origin, the lipid concentrations were normalized with lipid phosphate, which was determined using a total phosphorous assay (58).

HPTLC

The extracted lipids were dissolved in C/M (2:1, v/v), applied to a HPTLC plate (Silica Gel 60; Merck Millipore) or a HPTLC plate impregnated with 1% boric acid, and developed with C/M/W (65:35:8, v/v/v) or hexane/isopropyl alcohol/C/M/W (25:35:65:25:3, v/v/v/v/v). The carbohydrate portion of the lipids was visualized with orcinol reagent (120 °C, 10 min). β-GlcChol, GlcCer, and GalCer were identified by co-migration with their respective commercial standards, such as β-GlcChol, GlcCer (d18:1-C18:0), and GalCer from bovine brain. β-GalChol was identified by co-migration with its synthetic standard.

siRNA delivery and transfection

For RNA-mediated interference (RNAi) experiments, we used Stealth RNAi™ siRNAs (Thermo Fisher Scientific) carrying the following sequences: 5′-CCCAUCCAGGCUAAUCACACGGGCA-3′ (sense) and 5′-UGCCCGUGUGAUUAGCCUGGAUGGG-3′ (antisense) for GBA1; 5′-CCUGAAGUUUGUGCUGCAGGUUUAU-3′ (sense) and 5′-AUAAACCUGCAGCACAAACUUCAGG-3′ (antisense) for GBA2; 5′-GGUAUCAGCUCAUACCACUCAGUUU-3′ (sense) and 5′-AAACUGAGUGGUAUGAGCUGAUACC-3′ (antisense) for GALC; and 5′-CAGCGCUACCCAGGGAUCUUUAACA-3′ (sense) and 5′-UGUUAAAGAUCCCUGGGUAGCGCUG-3′ (antisense) for CGT. Stealth RNAi™ siRNA negative control was obtained from Thermo Fisher Scientific. siRNAs were delivered with Lipofectamine™ RNAiMAX transfection reagent (Thermo Fisher Scientific) according to the manufacturer's instructions. After incubation for 72 h, medium containing transfection reagents was removed, and cells were harvested using standard methods after first washing with PBS. The cells were then subjected to lipid extraction.

To obtain material for Western blotting, the harvested cells were incubated with lysis buffer (20 mM Tris-HCl, 150 mM NaCl, 1 mM EDTA, 1% Nonidet P-40, 0.1% sodium deoxycholate, 0.1% SDS, 1 tablet/10 ml cOmplete™ Mini EDTA-free protease inhibitor mixture (pH 7.4) (Roche Applied Science, Basel, Switzerland)) for 5 min at 4 °C, and then centrifuged at 18,000 × *g* for 30 min at 4 °C. The obtained supernatants were processed for Western blotting.

Exosome isolation

Exosomes were prepared from culture supernatants of H4 cells and mouse primary cortical neurons as described previously (26). For H4 cells, culture medium was replaced with serum-free medium 1 day before exosome isolation; culture supernatants were collected 24 h later. For the primary cortical neurons, culture supernatants were collected according to the method described under "Cell cultures." The collected culture supernatants were sequentially centrifuged at 3,000 × *g* for 10 min at 4 °C, 4,000 × *g* for 10 min at 4 °C, and 10,000 × *g* for 30 min at 4 °C to remove cells, dead cells, and debris. To obtain exosomes as pellets, the material was centrifuged again at 100,000 × *g* for 1 h at 4 °C. The resulting pellets were then subjected to lipid extraction, particle size analysis, and sucrose gradient centrifugation.

For sucrose gradient centrifugation, each exosome pellet was suspended with 1 ml of 2.3 M sucrose in 20 mM HEPES and transferred into centrifugal tubes (Ultra-Clear™, 14 × 89 mm; Beckman Coulter K.K., Tokyo, Japan). The sucrose gradient (11 ml of 0.25–2.3 M sucrose in 20 mM HEPES) was subsequently layered onto 1 ml of resuspended exosomes and then centri-

fuged in an SW41TI swinging rotor (Beckman Coulter K.K.) at 100,000 × *g* for 18 h at 4 °C. After centrifugation, fractions of 1 ml (typically 11–12 fractions in total) were collected from the top layer of the gradient, diluted with ~2 ml of 20 mM HEPES, and pelleted by centrifugation for 1 h at 100,000 × *g*. The resulting pellets were resuspended in PBS and subjected to Western blotting.

Analysis of exosomal particle size

A qNano System (Izon Science, Ltd., Christchurch, New Zealand) was used to analyze the particle size of H4− and mouse primary cortical neuron-derived exosomes resuspended in 50 mM HEPES, 150 mM KCl (pH 8.0). We followed the manufacturer's instructions.

Western blotting

Extracted proteins from cell lysates and exosomes were subjected to SDS-PAGE followed by Western blotting. The protein concentration was determined by a Pierce™ BCA protein assay kit (Thermo Fisher Scientific). Typically, proteins present in the cell lysates were separated by SDS-PAGE and transferred to a polyvinylidene difluoride membrane (Bio-Rad). We used the following primary antibodies in separate detections with the indicated dilutions: anti-GBA1 (catalogue no. G4171, Sigma-Aldrich; 1:1,000 dilution); anti-GBA2 (catalogue no. ab205064, Abcam, Cambridge, MA; 1:200 dilution); anti-GALC (catalogue no. sc-67352, Santa Cruz Biotechnology, Inc., Dallas, TX; 1:200 dilution); anti-CGT (catalogue no. sc-292071, Santa Cruz Biotechnology, Inc.; 1:200 dilution); anti-β-actin (catalogue no. PM053, Medical and Biological Laboratories Co., Ltd., Nagoya, Japan; 1:10,000 dilution); anti-GM130 (catalogue no. 610822, BD Biosciences; 1:1,000 dilution); anti-KDEL (catalogue no. PM059, Medical and Biological Laboratories Co., Ltd.; 1:1,000 dilution); anti-Alix (catalogue no. sc-53538, Santa Cruz Biotechnology, Inc.; 1:200 dilution); anti-tsg101 (catalogue no. sc-7964, Santa Cruz Biotechnology, Inc.; 1:200 dilution); and anti-flotillin-1 (catalogue no. 610820, BD Biosciences; 1:1,000 dilution). KDEL is an ER retention sequence. Alix (ALG-2 interacting protein X) is a cytoplasmic protein and is concentrated in exosomes. Tsg101 is a tumor susceptibility gene 101 protein and is concentrated in exosomes.

For secondary antibodies, we used the following: horseradish peroxidase (HRP)-conjugated anti-rabbit IgG (catalogue no. 170-6515, Bio-Rad; 1:20,000 dilution) or HRP-conjugated anti-mouse IgG (catalogue no. 170-6516, Bio-Rad; 1:20,000 dilution). Immunovisualization was performed using an enhanced chemiluminescence system (Nacalai Tesque).

In vitro assay of transglycosylase activity

The transglycosylase assay was carried out according to the method we established previously (59), with slight modifications. The reaction mixture in a total volume of 20 μl contained 40 μM NBD–chol, 80 or 200 μM glycolipid donor (GlcCer (d18:1-C18:1), GalCer (d18:1-C12:0), GlcSph, or GalSph), or 360 μM UDP-Gal dissolved in appropriate buffer, 2% ethanol, and a desired amount of enzyme. The assay for rGBA1 was performed with 10 μl of McIlvaine buffer (pH 5.3) and CHAPS (final 0.5%, w/v) (Dojindo, Kumamoto, Japan). The assay for the homogenate of human GBA2-expressing HEK293T cells was performed with 15.9 μl of McIlvaine buffer (pH 5.8) containing 0.1% (w/v) BSA. According to the method described in Ref. 56, the assay for rGALC was performed with 10 μl of McIlvaine buffer (pH 4.1), CHAPS (final 0.5%, w/v), Triton X-100 (final 0.01–0.02%, v/v), oleic acid (final 2 μg/μl), and sodium taurocholate (final 7 μg/μl). After incubation at 37 °C for 2 h, the reaction was terminated by adding chloroform/methanol (2:1, v/v), and the lipids were extracted and analyzed as reported previously (59).

The assay of transglycosylase activity was also performed with natural cholesterol as the acceptor. The reaction mixture in a total volume of 40 μl contained 40 μM cholesterol, 80 or 200 μM GalCer (d18:1-C12:0) dissolved in the appropriate buffer as described above, 2% ethanol, and a desired amount of enzyme. The volume of McIlvaine buffer in the reaction mixture was 2× greater than described above. After incubation at 37 °C for 2 h, the reaction was terminated by adding chloroform/methanol (2:1, v/v) containing 800 fmol of β-GlcChol-d_7 as an internal standard to normalize extraction efficiency. Lipid extraction was performed by Folch's partition, and the organic phase was pooled and evaporated. The extracted lipids were separated by HPTLC with chloroform/methanol (85:15, v/v). Lipids were stained with primuline reagent and visualized using long-wave UV. The bands co-migrating with standard β-GlcChol and β-GalChol were collected, combined, and extracted using Folch's partition. The organic layer containing sterylglycosides was collected and dried under a stream of N_2. The extracted lipids were subjected to HILIC–ESI–MS/MS, and formation of β-GalChol was determined.

In vitro assay of GlcCer or GalCer hydrolase activity

The GlcCer and GalCer hydrolase assay used in this study was carried out according to the method we described previously (16), with some modifications. The reaction mixture in a total volume of 20 μl contained 100 pmol of C_6-NBD–GlcCer or C_6-NBD–GalCer dissolved in appropriate buffer and a desired amount of enzyme. The assay for rGBA1 was performed with 10 μl of McIlvaine buffer (pH 5.3), Triton X-100 (final 0.25%, v/v), and sodium taurocholate (final 0.6%, w/v). The assay for the homogenate of human GBA2-expressing HEK293T cells was performed with 16.6 μl of McIlvaine buffer (pH 5.8) containing 0.1% (w/v) BSA and ethanol (final 1%). The assay for rGALC was performed with 10 μl of McIlvaine buffer (pH 4.1), Triton X-100 (final 0.01%, v/v), oleic acid (final 2 μg/μl), and sodium taurocholate (final 7 μg/μl). After incubation at 37 °C for 30 min, the reaction was terminated by adding chloroform/methanol (2:1, v/v); the lipids were extracted, and C_6-NBD–ceramide formation was analyzed as reported before (16).

Statistical analysis

Statistical analyses and univariate descriptive statistics were performed using GraphPad Prism, version 5.02 for Windows (GraphPad Software, San Diego, CA). Group means ± S.E. was calculated. To assess group differences, at least three independent experiments were assessed using unpaired *t* tests.

Author contributions—H. A. and Y. H. conceptualization; H. A. data curation; H. A., H. K., R. T., and Y. H. funding acquisition; H. A., M. I., Y. N., T. S., K. Y., Y. Y., P. G., and Y. H. investigation; H. A. methodology; H. A., E. N., Y. Y., and P. G. writing-original draft; H. A. and Y. H. project administration; H. A., E. N., N. U., K. Y., Y. Y., H. K., R. T., J. M. A., P. G., and Y. H. writing-review and editing; E. N., N. U., R. T., and J. M. A. resources; H. K., J. M. A., P. G., and Y. H. supervision.

Acknowledgments—We thank the Support Unit for Bio-Material Analysis, Research Resources Division, RIKEN Center for Brain Science, with special thanks to A. A., K. O., and M. U. for the MALDI-TOF/TOF analysis. We also thank the Molecular Structure Characterization Unit, RIKEN Center for Sustainable Resource Science, with special thanks to T. N. for the GC/MS analysis.

References

1. Grille, S., Zaslawski, A., Thiele, S., Plat, J., and Warnecke, D. (2010) The functions of steryl glycosides come to those who wait: recent advances in plants, fungi, bacteria, and animals. *Prog. Lipid Res.* **49,** 262–288 CrossRef Medline
2. Marques, A. R., Mirzaian, M., Akiyama, H., Wisse, P., Ferraz, M. J., Gaspar, P., Ghauharali-van der Vlugt, K., Meijer, R., Giraldo, P., Alfonso, P., Irún, P., Dahl, M., Karlsson, S., Pavlova, E. V., *et al.* (2016) Glucosylated cholesterol in mammalian cells and tissues: formation and degradation by multiple cellular β-glucosidases. *J. Lipid Res.* **57,** 451–463 CrossRef Medline
3. Akiyama, H., Nakajima, K., Itoh, Y., Sayano, T., Ohashi, Y., Yamaguchi, Y., Greimel, P., and Hirabayashi, Y. (2016) Aglycon diversity of brain sterylglucosides: structure determination of cholesteryl- and sitosterylglucoside. *J. Lipid Res.* **57,** 2061–2072 CrossRef Medline
4. Brady, R. O., Kanfer, J. N., and Shapiro, D. (1965) Metabolism of glucocerebrosides. II. Evidence of an enzymatic deficiency in Gaucher's disease. *Biochem. Biophys. Res. Commun.* **18,** 221–225 CrossRef Medline
5. Hruska, K. S., LaMarca, M. E., Scott, C. R., and Sidransky, E. (2008) Gaucher disease: mutation and polymorphism spectrum in the glucocerebrosidase gene (GBA). *Hum. Mutat.* **29,** 567–583 CrossRef Medline
6. Sidransky, E., Nalls, M. A., Aasly, J. O., Aharon-Peretz, J., Annesi, G., Barbosa, E. R., Bar-Shira, A., Berg, D., Bras, J., Brice, A., Chen, C. M., Clark, L. N., Condroyer, C., De Marco, E. V., Dürr, A., *et al.* (2009) Multicenter analysis of glucocerebrosidase mutations in Parkinson's disease. *N. Engl. J. Med.* **361,** 1651–1661 CrossRef Medline
7. Mitsui, J., Matsukawa, T., Sasaki, H., Yabe, I., Matsushima, M., Dürr, A., Brice, A., Takashima, H., Kikuchi, A., Aoki, M., Ishiura, H., Yasuda, T., Date, H., Ahsan, B., Iwata, A., *et al.* (2015) Variants associated with Gaucher disease in multiple system atrophy. *Ann. Clin. Transl. Neurol.* **2,** 417–426 CrossRef Medline
8. van Weely, S., Brandsma, M., Strijland, A., Tager, J. M., and Aerts, J. M. (1993) Demonstration of the existence of a second, non-lysosomal glucocerebrosidase that is not deficient in Gaucher disease. *Biochim. Biophys. Acta* **1181,** 55–62 CrossRef Medline
9. Yildiz, Y., Matern, H., Thompson, B., Allegood, J. C., Warren, R. L., Ramirez, D. M., Hammer, R. E., Hamra, F. K., Matern, S., and Russell, D. W. (2006) Mutation of β-glucosidase 2 causes glycolipid storage disease and impaired male fertility. *J. Clin. Invest.* **116,** 2985–2994 CrossRef Medline
10. Boot, R. G., Verhoek, M., Donker-Koopman, W., Strijland, A., van Marle, J., Overkleeft, H. S., Wennekes, T., and Aerts, J. M. (2007) Identification of the non-lysosomal glucosylceramidase as β-glucosidase 2. *J. Biol. Chem.* **282,** 1305–1312 CrossRef Medline
11. Körschen, H. G., Yildiz, Y., Raju, D. N., Schonauer, S., Bönigk, W., Jansen, V., Kremmer, E., Kaupp, U. B., and Wachten, D. (2013) The non-lysosomal β-glucosidase GBA2 is a non-integral membrane-associated protein at the endoplasmic reticulum (ER) and Golgi. *J. Biol. Chem.* **288,** 3381–3393 CrossRef Medline
12. Gonzalez-Carmona, M. A., Sandhoff, R., Tacke, F., Vogt, A., Weber, S., Canbay, A. E., Rogler, G., Sauerbruch, T., Lammert, F., and Yildiz, Y. (2012) β-Glucosidase 2 knockout mice with increased glucosylceramide show impaired liver regeneration. *Liver Int.* **32,** 1354–1362 CrossRef Medline
13. Hammer, M. B., Eleuch-Fayache, G., Schottlaender, L. V., Nehdi, H., Gibbs, J. R., Arepalli, S. K., Chong, S. B., Hernandez, D. G., Sailer, A., Liu, G., Mistry, P. K., Cai, H., Shrader, G., Sassi, C., Bouhlal, Y., *et al.* (2013) Mutations in GBA2 cause autosomal-recessive cerebellar ataxia with spasticity. *Am. J. Hum. Genet.* **92,** 245–251 CrossRef Medline
14. Martin, E., Schüle, R., Smets, K., Rastetter, A., Boukhris, A., Loureiro, J. L., Gonzalez, M. A., Mundwiller, E., Deconinck, T., Wessner, M., Jornea, L., Oteyza, A. C., Durr, A., Martin, J. J., Schöls, L., *et al.* (2013) Loss of function of glucocerebrosidase GBA2 is responsible for motor neuron defects in hereditary spastic paraplegia. *Am. J. Hum. Genet.* **92,** 238–244 CrossRef Medline
15. Votsi, C., Zamba-Papanicolaou, E., Middleton, L. T., Pantzaris, M., and Christodoulou, K. (2014) A novel GBA2 gene missense mutation in spastic ataxia. *Ann. Hum. Genet.* **78,** 13–22 CrossRef Medline
16. Akiyama, H., Kobayashi, S., Hirabayashi, Y., and Murakami-Murofushi, K. (2013) Cholesterol glucosylation is catalyzed by transglucosylation reaction of β-glucosidase 1. *Biochem. Biophys. Res. Commun.* **441,** 838–843 CrossRef Medline
17. Diekman, J., and Djerassi, C. (1967) Mass spectrometry in structural and stereochemical problems. CXXV. Mass spectrometry of some steroid trimethylsilyl ethers. *J. Org. Chem.* **32,** 1005–1012 CrossRef Medline
18. Nakajima, K., Akiyama, H., Tanaka, K., Kohyama-Koganeya, A., Greimel, P., and Hirabayashi, Y. (2016) Separation and analysis of mono-glucosylated lipids in brain and skin by hydrophilic interaction chromatography based on carbohydrate and lipid moiety. *J. Chromatogr. B. Analyt. Technol. Biomed. Life Sci.* **1031,** 146–153 CrossRef Medline
19. von Gerichten, J., Schlosser, K., Lamprecht, D., Morace, I., Eckhardt, M., Wachten, D., Jennemann, R., Gröne, H. J., Mack, M., and Sandhoff, R. (2017) Diastereomer-specific quantification of bioactive hexosylceramides from bacteria and mammals. *J. Lipid Res.* **58,** 1247–1258 CrossRef Medline
20. Akiyama, H., Hamada, T., Nagatsuka, Y., Kobayashi, S., Hirabayashi, Y., and Murakami-Murofushi, K. (2011) A possible mechanism of cholesteryl glucoside formation involved in heat shock response in the animal cell membrane. *Cytologia* **76,** 19–25 CrossRef
21. Wubbolts, R., Leckie, R. S., Veenhuizen, P. T., Schwarzmann, G., Möbius, W., Hoernschemeyer, J., Slot, J. W., Geuze, H. J., and Stoorvogel, W. (2003) Proteomic and biochemical analyses of human B cell-derived exosomes. Potential implications for their function and multivesicular body formation. *J. Biol. Chem.* **278,** 10963–10972 CrossRef Medline
22. Brügger, B., Glass, B., Haberkant, P., Leibrecht, I., Wieland, F. T., and Kräusslich, H. G. (2006) The HIV lipidome: a raft with an unusual composition. *Proc. Natl. Acad. Sci. U.S.A.* **103,** 2641–2646 CrossRef Medline
23. Trajkovic, K., Hsu, C., Chiantia, S., Rajendran, L., Wenzel, D., Wieland, F., Schwille, P., Brügger, B., and Simons, M. (2008) Ceramide triggers budding of exosome vesicles into multivesicular endosomes. *Science* **319,** 1244–1247 CrossRef Medline
24. Skotland, T., Sandvig, K., and Llorente, A. (2017) Lipids in exosomes: current knowledge and the way forward. *Prog. Lipid Res.* **66,** 30–41 CrossRef Medline
25. Simons, M., and Raposo, G. (2009) Exosomes–vesicular carriers for intercellular communication. *Curr. Opin. Cell Biol.* **21,** 575–581 CrossRef Medline
26. Yuyama, K., Sun, H., Mitsutake, S., and Igarashi, Y. (2012) Sphingolipid-modulated exosome secretion promotes clearance of amyloid-β by microglia. *J. Biol. Chem.* **287,** 10977–10989 CrossRef Medline
27. Yuyama, K., Sun, H., Sakai, S., Mitsutake, S., Okada, M., Tahara, H., Furukawa, J., Fujitani, N., Shinohara, Y., and Igarashi, Y. (2014) Decreased amyloid-β pathologies by intracerebral loading of glycosphingolipid-enriched exosomes in Alzheimer model mice. *J. Biol. Chem.* **289,** 24488–24498 CrossRef Medline

28. Yamaji, T., and Hanada, K. (2014) Establishment of HeLa cell mutants deficient in sphingolipid-related genes using TALENs. *PLoS ONE* **9,** e88124 CrossRef Medline
29. Sleat, D. E., Wiseman, J. A., El-Banna, M., Price, S. M., Verot, L., Shen, M. M., Tint, G. S., Vanier, M. T., Walkley, S. U., and Lobel, P. (2004) Genetic evidence for nonredundant functional cooperativity between NPC1 and NPC2 in lipid transport. *Proc. Natl. Acad. Sci. U.S.A.* **101,** 5886–5891 CrossRef Medline
30. Ory, D. S. (2000) Niemann-Pick type C: a disorder of cellular cholesterol trafficking. *Biochim. Biophys. Acta* **1529,** 331–339 CrossRef Medline
31. Marques, A. R., Aten, J., Ottenhoff, R., van Roomen, C. P., Herrera Moro, D., Claessen, N., Vinueza Veloz, M. F., Zhou, K., Lin, Z., Mirzaian, M., Boot, R. G., De Zeeuw, C. I., Overkleeft, H. S., Yildiz, Y., and Aerts, J. M. (2015) Reducing GBA2 activity ameliorates neuropathology in Niemann-Pick type C mice. *PLoS ONE* **10,** e0135889 CrossRef Medline
32. Ben-Menachem, G., Kubler-Kielb, J., Coxon, B., Yergey, A., and Schneerson, R. (2003) A newly discovered cholesteryl galactoside from *Borrelia burgdorferi*. *Proc. Natl. Acad. Sci. U.S.A.* **100,** 7913–7918 CrossRef Medline
33. Schröder, N. W., Schombel, U., Heine, H., Göbel, U. B., Zähringer, U., and Schumann, R. R. (2003) Acylated cholesteryl galactoside as a novel immunogenic motif in *Borrelia burgdorferi* sensu stricto. *J. Biol. Chem.* **278,** 33645–33653 CrossRef Medline
34. Baumann, N. A., Harpin, M. L., and Bourré, J. M. (1970) Long chain fatty acid formation: key step in myelination studied in mutant mice. *Nature* **227,** 960–961 CrossRef Medline
35. Ly, P. T., Pelech, S., and Shaw, C. A. (2008) Cholesteryl glucoside stimulates activation of Protein kinase B/Akt in the motor neuron-derived NSC34 cell line. *Neurobiol. Lipids* **7,** 620081 Medline
36. Khabazian, I., Bains, J. S., Williams, D. E., Cheung, J., Wilson, J. M., Pasqualotto, B. A., Pelech, S. L., Andersen, R. J., Wang, Y. T., Liu, L., Nagai, A., Kim, S. U., Craig, U. K., and Shaw, C. A. (2002) Isolation of various forms of sterol β-D-glucoside from the seed of *Cycas circinalis*: neurotoxicity and implications for ALS-parkinsonism dementia complex. *J. Neurochem.* **82,** 516–528 CrossRef Medline
37. Tabata, R. C., Wilson, J. M., Ly, P., Zwiegers, P., Kwok, D., Van Kampen, J. M., Cashman, N., and Shaw, C. A. (2008) Chronic exposure to dietary sterol glucosides is neurotoxic to motor neurons and induces an ALS-PDC phenotype. *Neuromolecular Med.* **10,** 24–39 CrossRef Medline
38. Wilson, J. M., Khabazian, I., Wong, M. C., Seyedalikhani, A., Bains, J. S., Pasqualotto, B. A., Williams, D. E., Andersen, R. J., Simpson, R. J., Smith, R., Craig, U. K., Kurland, L. T., and Shaw, C. A. (2002) Behavioral and neurological correlates of ALS-parkinsonism dementia complex in adult mice fed washed cycad flour. *Neuromolecular Med.* **1,** 207–221 CrossRef Medline
39. Van Kampen, J. M., Baranowski, D. C., Robertson, H. A., Shaw, C. A., and Kay, D. G. (2015) The progressive BSSG rat model of Parkinson's: recapitulating multiple key features of the human disease. *PLoS ONE* **10,** e0139694 CrossRef Medline
40. Maas, S. L. N., Breakefield, X. O., and Weaver, A. M. (2017) Extracellular vesicles: unique intercellular delivery vehicles. *Trends Cell Biol.* **27,** 172–188 CrossRef Medline
41. Ghisaidoobe, A. T., van den Berg, R. J., Butt, S. S., Strijland, A., Donker-Koopman, W. E., Scheij, S., van den Nieuwendijk, A. M., Koomen, G. J., van Loevezijn, A., Leemhuis, M., Wennekes, T., van der Stelt, M., van der Marel, G. A., van Boeckel, C. A., Aerts, J. M., and Overkleeft, H. S. (2014) Identification and development of biphenyl substituted iminosugars as improved dual glucosylceramide synthase/neutral glucosylceramidase inhibitors. *J. Med. Chem.* **57,** 9096–9104 CrossRef Medline
42. Charoenwattanasatien, R., Pengthaisong, S., Breen, I., Mutoh, R., Sansenya, S., Hua, Y., Tankrathok, A., Wu, L., Songsiriritthigul, C., Tanaka, H., Williams, S. J., Davies, G. J., Kurisu, G., and Cairns, J. R. (2016) Bacterial β-glucosidase reveals the structural and functional basis of genetic defects in human glucocerebrosidase 2 (GBA2). *ACS Chem. Biol.* **11,** 1891–1900 CrossRef Medline
43. Sprong, H., Kruithof, B., Leijendekker, R., Slot, J. W., van Meer, G., and van der Sluijs, P. (1998) UDP-galactose:ceramide galactosyltransferase is a class I integral membrane protein of the endoplasmic reticulum. *J. Biol. Chem.* **273,** 25880–25888 CrossRef Medline
44. Nagano, S., Yamada, T., Shinnoh, N., Furuya, H., Taniwaki, T., and Kira, J. (1998) Expression and processing of recombinant human galactosylceramidase. *Clin. Chim. Acta* **276,** 53–61 CrossRef Medline
45. Burger, K. N., van der Bijl, P., and van Meer, G. (1996) Topology of sphingolipid galactosyltransferases in ER and Golgi: transbilayer movement of monohexosyl sphingolipids is required for higher glycosphingolipid biosynthesis. *J. Cell Biol.* **133,** 15–28 CrossRef Medline
46. Grabowski, G. A., Barton, N. W., Pastores, G., Dambrosia, J. M., Banerjee, T. K., McKee, M. A., Parker, C., Schiffmann, R., Hill, S. C., and Brady, R. O. (1995) Enzyme therapy in type 1 Gaucher disease: comparative efficacy of mannose-terminated glucocerebrosidase from natural and recombinant sources. *Ann. Intern. Med.* **122,** 33–39 CrossRef Medline
47. Dvir, H., Harel, M., McCarthy, A. A., Toker, L., Silman, I., Futerman, A. H., and Sussman, J. L. (2003) X-ray structure of human acid-β-glucosidase, the defective enzyme in Gaucher disease. *EMBO Rep.* **4,** 704–709 CrossRef Medline
48. Loftus, S. K., Morris, J. A., Carstea, E. D., Gu, J. Z., Cummings, C., Brown, A., Ellison, J., Ohno, K., Rosenfeld, M. A., Tagle, D. A., Pentchev, P. G., and Pavan, W. J. (1997) Murine model of Niemann-Pick C disease: mutation in a cholesterol homeostasis gene. *Science* **277,** 232–235 CrossRef Medline
49. Uemura, N., Koike, M., Ansai, S., Kinoshita, M., Ishikawa-Fujiwara, T., Matsui, H., Naruse, K., Sakamoto, N., Uchiyama, Y., Todo, T., Takeda, S., Yamakado, H., and Takahashi, R. (2015) Viable neuronopathic Gaucher disease model in Medaka (*Oryzias latipes*) displays axonal accumulation of α-synuclein. *PLoS Genet.* **11,** e1005065 CrossRef Medline
50. Keatinge, M., Bui, H., Menke, A., Chen, Y. C., Sokol, A. M., Bai, Q., Ellett, F., Da Costa, M., Burke, D., Gegg, M., Trollope, L., Payne, T., McTighe, A., Mortiboys, H., de Jager, S., Nuthall, H., *et al.* (2015) Glucocerebrosidase 1 deficient *Danio rerio* mirror key pathological aspects of human Gaucher disease and provide evidence of early microglial activation preceding α-synuclein-independent neuronal cell death. *Hum. Mol. Genet.* **24,** 6640–6652 CrossRef Medline
51. Zancan, I., Bellesso, S., Costa, R., Salvalaio, M., Stroppiano, M., Hammond, C., Argenton, F., Filocamo, M., and Moro, E. (2015) Glucocerebrosidase deficiency in zebrafish affects primary bone ossification through increased oxidative stress and reduced Wnt/β-catenin signaling. *Hum. Mol. Genet.* **24,** 1280–1294 CrossRef Medline
52. Ansai, S., and Kinoshita, M. (2014) Targeted mutagenesis using CRISPR/Cas system in medaka. *Biol. Open* **3,** 362–371 CrossRef Medline
53. Ichikawa, S., Sakiyama, H., Suzuki, G., Hidari, K. I., and Hirabayashi, Y. (1996) Expression cloning of a cDNA for human ceramide glucosyltransferase that catalyzes the first glycosylation step of glycosphingolipid synthesis. *Proc. Natl. Acad. Sci. U.S.A.* **93,** 4638–4643 CrossRef Medline
54. Lahav, D., Liu, B., van den Berg, R. J. B. H. N., van den Nieuwendijk, A. M. C. H., Wennekes, T., Ghisaidoobe, A. T., Breen, I., Ferraz, M. J., Kuo, C. L., Wu, L., Geurink, P. P., Ovaa, H., van der Marel, G. A., van der Stelt, M., Boot, R. G., *et al.* (2017) A fluorescence polarization activity-based protein profiling assay in the discovery of potent, selective inhibitors for human nonlysosomal glucosylceramidase. *J. Am. Chem. Soc.* **139,** 14192–14197 CrossRef Medline
55. Folch, J., Lees, M., and Sloane Stanley, G. H. (1957) A simple method for the isolation and purification of total lipides from animal tissues. *J. Biol. Chem.* **226,** 497–509 Medline
56. Raghavan, S., and Krusell, A. (1986) Optimal assay conditions for enzymatic characterization of homozygous and heterozygous twitcher mouse. *Biochim. Biophys. Acta* **877,** 1–8 CrossRef Medline
57. Bligh, E. G., and Dyer, W. J. (1959) A rapid method of total lipid extraction and purification. *Can. J. Biochem. Physiol.* **37,** 911–917 CrossRef Medline
58. Fiske, C. H., and Subbarow, Y. (1925) The colorimetric determination of phosphorus. *J. Biol. Chem.* **66,** 375–400
59. Akiyama, H., Sasaki, N., Hanazawa, S., Gotoh, M., Kobayashi, S., Hirabayashi, Y., and Murakami-Murofushi, K. (2011) Novel sterol glucosyltransferase in the animal tissue and cultured cells: evidence that glucosylceramide as glucose donor. *Biochim. Biophys. Acta* **1811,** 314–322 CrossRef Medline